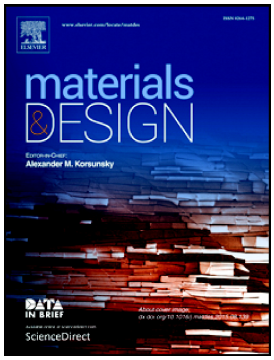

Defect-free TiC/Si multi-layer electrical discharge coatings

J.W. Murray, R.B. Cook, N. Senin, S.J. Algodi, A.T. Clare

PII: S0264-1275(18)30486-6
DOI: doi:10.1016/j.matdes.2018.06.019
Reference: JMADE 3989

To appear in: *Materials & Design*

Received date: 19 March 2018
Revised date: 24 May 2018
Accepted date: 10 June 2018

Please cite this article as: J.W. Murray, R.B. Cook, N. Senin, S.J. Algodi, A.T. Clare , Defect-free TiC/Si multi-layer electrical discharge coatings. Jmade (2017), doi:10.1016/j.matdes.2018.06.019

Defect-free TiC/Si multi-layer electrical discharge coatings

J.W. Murray[1], R.B. Cook[3], N. Senin[1], S.J. Algodi[1,4], A.T. Clare[1,2]*

[1]Department of M3, Faculty of Engineering, University of Nottingham, University Park, Nottingham, NG7 2RD, UK

[2]Department of Mechanical, Materials and Manufacturing Engineering, Faculty of Science and Engineering, University of Nottingham China, 199 Taikang East Road, University Park, Ningbo 315100, China

[3]National Centre for Advanced Tribology (nCATS), School of Engineering Sciences, Highfield Campus, Southampton, SO17 1EU, UK

[3]Department of Mechanical Engineering, College of Engineering, Al-Nahrain University, Baghdad, Iraq

Abstract

The process of electrical discharge coating (EDC) may be used to deposit hard materials on conformal substrate surfaces. Next generation EDM'd components may exploit attachment phenomena to enhance recast layer properties, to avoid the need for recast layer removal. Here, a ceramic based composite layer was developed without cracking and porosity for the first time, using sequential coating using sacrificial TiC and Si electrodes. Attenuation of the discharge process by gap widening using Si debris in the gap explained improved layer properties. Composite coatings combining WC and TiC were also demonstrated, with good elemental intermixing. Attachment level was correlated strongly with melting point, with high melting point materials resisting ejection due to more rapid solidification. Nanoindentation showed the TiC and WC/TiC layers possessed the highest mean hardness

values, approximately double that of the Cu based machined layer which itself yielded a much higher hardness of 11.0 GPa compared to 1.9 GPa of the substrate.

Keywords: electrical discharge coating; nanohardness; EDM; cracking; porosity; TiC

1. Introduction

Electrical discharge coating (EDC) is a surface modification process used to produce coatings from tool electrodes, or powder suspended in a dielectric fluid, onto a target workpiece surface. The EDC process exploits the principle of sparking, being an adaptation of electrical discharge machining (EDM), to deposit functionally significant amounts of material on to complex shapes and uneven surfaces, as part of an integrated manufacturing process. A combination of negative tool polarity, high gap voltages, short pulse on-times and long pulse-off times acts to intensify material adhesion. The high temperatures associated with sparking allow a large range of difficult to process materials to be deposited, including ceramics, and rapid quenching facilitates the production of hard coatings [1, 2]. The next generation of ED machining may exploit the phenomena associated with EDC and attachment of desirable materials to neutralise and enhance the properties of the undesirable recast layer.

One advantage of EDC is that it is well suited to the production of high melting point material ceramic coatings onto any kind of electrically conductive substrate. However, hard ceramics, such as TiC, exhibit much higher melting points and much lower thermal expansion coefficients than most metals and metallic alloys. As a result, such ED coatings are often characterised by high levels of cracking and porosity. Practical applications for EDC are limited presently by the poor integrity of the processed surfaces. For example, TiC coatings produced from titanium/graphite sandwiched electrodes exhibited rough surfaces

with porosity and cracking [3]. Similarly, coatings of TiC produced from Ti particles suspended in oil were characterised by cracking and porosity [4]. Porosity associated with EDM and EDC processed materials is attributed generally to the presence of gas trapped within molten layers developed by the ED process. The proliferation of cracks is thought to occur by aggressive sparking conditions, or by the development of multiple phases with differing thermal expansion coefficients [5]. It has been shown that the presence of porosity worsens the delamination wear behaviour of iron, via stress concentrations and collection sites for wear debris [6]. A correlation between porosity and wear rate has also been shown also for bulk SiC/Cu composites [7]. Further, crack initiation and propagation is known to be the main failure mechanism of thermal barrier coatings subjected to thermomechanical loading [8], and crack initiated delamination is thought to be a common failure mechanism of thin films [9]. In this context, it is anticipated that reductions in cracking and porosity will yield ED coatings with improved fatigue and tribological properties, and hence enhanced part lifetimes.

In the authors' prior work, fundamental microstructural analysis was performed to reveal that a TiC based coating on a steel substrate comprises a complex, graded composite structure in which substrate material is drawn between TiC particles, forming a matrix [10]. Each individual deposit/discharge containing TiC results in a low level of movement of molten sub-meltpool substrate material towards the surface. Incrementally this level of substrate material increases until an equilibrium composite structure is reached. Given that the EDC process has been demonstrated effectively as a composite coating forming process, it is therefore well suited to form multi-layer coatings using sequential, varying coating materials.

EDC has continued to attract academic interest particularly for enhanced tribological properties, for example coatings from WS_2 and Cu powder electrodes yielded superior wear resistance compared to a mild steel substrate [11]. TiCN coatings formed from a titanium electrode and nitrogenous oil yielded lower wear than a TiN PVD coating at loads above 30 N [12]. Recently, a detailed wear study was performed using TiC based coatings from TiC powder metallurgy electrodes deposited onto types of steel substrate [13]. It was shown that due to the composite nature of the coating, the uptake of material from the substrate has a strong influence of the wear performance of the final coating, with coatings on the softer substrate yielding worse wear behaviour. In these TiC based coatings, cracking and porosity are prevalent and such defects are known to have a strong influence of mechanical properties. Individual coatings of TiC and Si were developed by Sumi et al. [14], with defects in the Si based coatings minimised. However, a convincing explanation for this phenomenon was not offered. ED multi-layer coatings created by sequential material deposition which incorporate the useful properties of both ceramic and Si based deposition have not been demonstrated in the literature. Here, we advance the state of the art of ED coatings by developing multi-layer coatings with an emphasis on TiC and WC for their potentially useful mechanical and tribological properties. Additionally, to further the understanding of attachment and coating formation during EDC, single layer coatings are developed which possess a large range of melting points, to determine the dependence of coating property and composition on material type. Nanoindentation data is reported also for the first time to reveal the hardness of such coatings in comparison to a typical EDM recast layer, thereby demonstrating potential practical properties for example for tooling, for which EDM is a commonly used technique.

2. Experimental

EDC coatings were developed on 304 stainless steel substrates, which were prepared by grinding and sequential mechanical polishing, with a final stage of 1 µm diamond grit, to give a mirror finish prior to coating (*Sa* roughness ~ 0.11 µm). This material was chosen as a substrate given it was a commonly used steel and it was also the material used in prior fundamental TEM work of the authors [10], and therefore this prior knowledge can be used to inform the present work. A Mitsubishi EA12V EDM machine was used for all coating experiments. A range of tool electrode materials (Table 1) was used initially for single layer coating trials, to appraise the effect of electrode material on coating development and morphology. TiC and WC material were manufactured by powder sintering. Cu, Zr and Si were in solid crystalline form. The EDC process time is determined by the tool electrode surface area, and hence the wear of sacrificial electrodes in the z-direction was used as a benchmark. The control of electrode wear amount also compensates for the varying electrode wear rates of the different materials, caused by their different melting points and/or manufacturing method. The EDC process parameter sets A and B, as identified from previous experimentation [15] and summarised in Table 1, were selected to promote tool electrode material transfer to the workpiece. Higher current conditions (Set A) were required to ensure the development of coatings of high temperature ceramics in a reasonable time scale. Lower current conditions (Set B) were associated with coatings exhibiting better surface finishes, whilst still permitting significant transfer of material to the workpiece. These parameter benchmarks (A and B) were developed originally based on the creation of TiC and Si coatings respectively with good levels of attachment.

Table 1 Experimental parameters

Tool electrode materials	TiC, Si, Cu, WC, Zr
Workpiece material	304 stainless steel

Oil (dielectric)	Shell Paraol 250
Tool electrode polarity	Negative
Parameter Set A	320 V; 10 A current: 8 µs ON / 256 µs OFF
Parameter Set B	260 V; 5.5 A current: 8 µs ON / 64 µs OFF

Scanning electron microscopy (SEM) was performed using Hitachi S2600N and FEI XL30 instruments in back-scattered electron (BSE) imaging mode in both plan and cross-sectional views. Energy-dispersive X-ray (EDX) analysis was performed using an Oxford Instruments INCA X-ray microanalysis system (20kV; working distance 10 mm). X-ray diffractometry (XRD) was performed using a Bruker AXS D500 in conventional $\theta/2\theta$ mode (Cu k_α (λ= 1.54060 Å); 40 kV; 25 mA; 0.02° step size; 8 s per step). Roughness values were obtained using an Alicona Infinite Focus G5 focus-variation microscope. *Sa* texture values (arithmetical mean height (ISO 25178-2), the 3D equivalent of arithmetical mean roughness *Ra* (ISO 4287)) were determined from areal data acquired using a 20× objective lens (working field of view (0.808 × 0.808) mm, pixel width (0.439 × 0.439) µm). For each topography data-set, four (0.4 × 0.4) mm regions were extracted and levelled by subtraction of the least-squares mean plane. The *Sa* parameter was computed on each region independently. Open-source image processing software ImageJ was used for the measurement of surface cracking and layer thicknesses from the BSE images. Surface cracking was determined by the manual tracing of cracks imaged in BSE mode for good contrast, using five images from each sample (1.5 mm^2 in total). Average layer thickness values were determined from 100 points of regular spacing along a 10 µm length of each coating, viewed in cross-section. Nano-indentation was performed using a Micromaterials NanoTest Vantage nano-indentation platform using a Diamond Berkovich indenter. 11 indents were performed in depth control to 150 nm at a rate of 0.1 mN/s with a 20 second

hold at maximum load. The indents were in the centre of the cross-sections of each sample and spaced 7 μm apart to ensure the plastic interaction volume was only within the coating and there was no overlap of the interaction volumes with the previous indents. ISO standard 14577 specifies that the thickness of material surrounding each indent should be greater than 10 times the maximum indentation depth, or 3 times the maximum indentation diameter, whichever is great, to avoid interaction effect with other indents [16]. Therefore with an indent diameter expected to be ten times the indent depth, this spacing was considered to be sufficient.

Hardness was calculated from by the division of maximum load by the projected area of contact.

Table 2 presents an overview of the sample sets investigated here. For example, the designation of WC/TiC refers to a coating made from an initial layer of WC followed by a layer of TiC.

Table 2 Coatings and parameter sets evaluated within this study

Electrode	Parameter Sets	Electrode wear (mm)
TiC, Si, Cu, WC, Zr	A	0.5
TiC, Si, Cu, WC, Zr	B	0.5
WC/TiC, TiC/WC	A / A	0.5 / 0.5
Si/TiC	B / A	0.2, 0.5, 1.0, 1.5 & 2.0 / 0.5
TiC/TiC	B / A	0.5 / 0.5
Si/TiC	B / A	0.5 / 0.5
TiC	A	Single discharge
Si	A	Single discharge
Si	B	Single discharge

3. Results

3.1 Single layer coating morphology

Single layer coatings were produced using TiC, Cu, Si, WC and Zr tool electrode materials, which possess a range of melting points (Table 3), to appraise the effect of thermal property on adhesion and coating surface characteristics. The coatings were produced using two sets of EDC parameters, corresponding to 'rough' (Set A) and 'fine' (Set B) discharge conditions (Table 1). In each case, 0.5 mm of material was worn from the tool electrode. Typical process time for each coating was 30 minutes, with coatings produced over an area of 100 mm^2. With TiC coatings produced using Set A parameters, approximately 5 million sparks in total affected the 100 mm^2 region, calculated from the average area of discharges and time taken for one discharge [15]. Representative SEM images of the TiC, Cu and Si coating surfaces are presented in Figure 1.

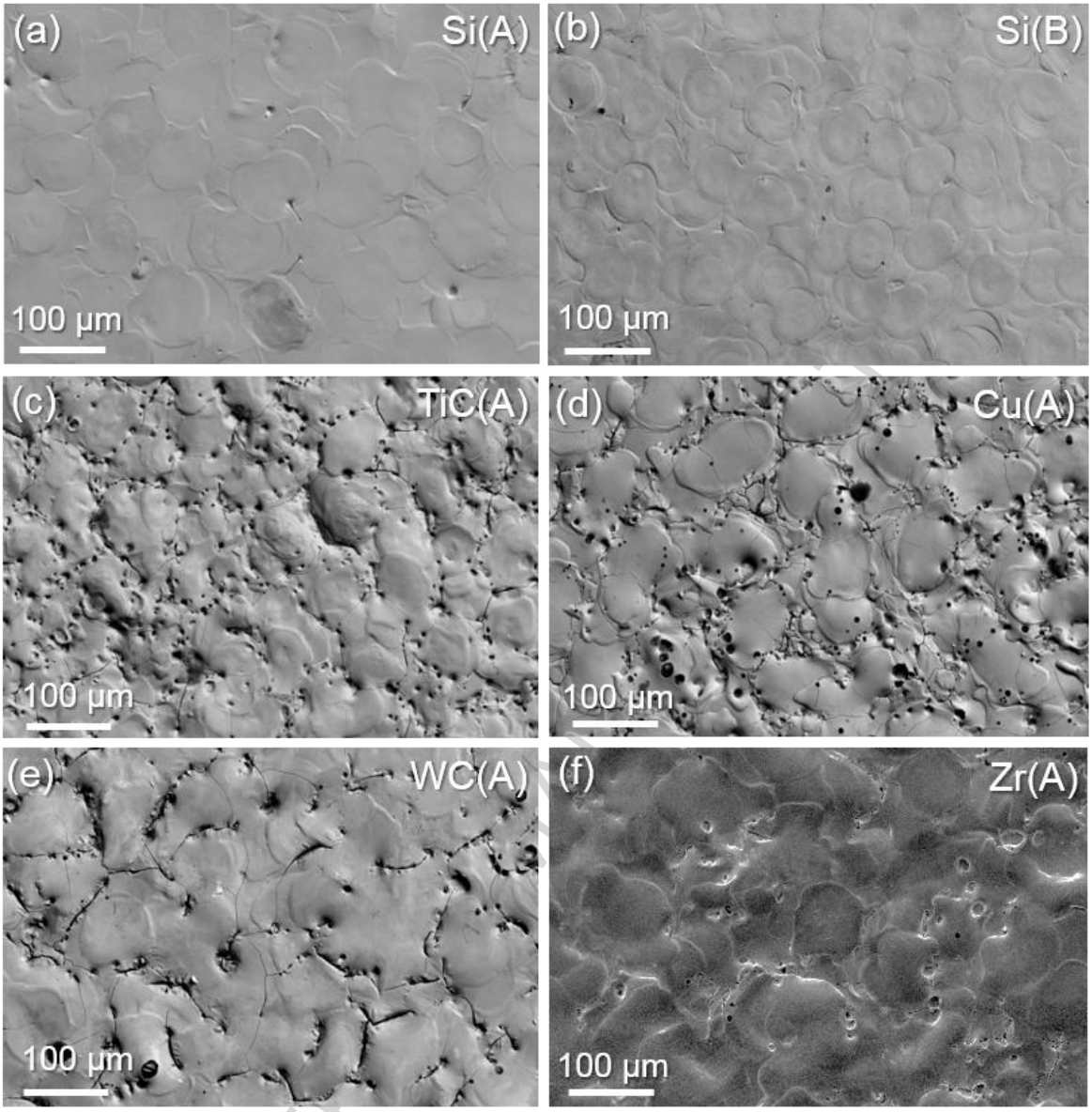

Figure 1 Surface morphology of various single layer coatings made using parameter set A, and silicon coating with parameter set B

All the developed coatings exhibited cracked and porous surfaces when produced using both parameter sets, with the exception of Si, which exhibited minimal levels of cracking and porosity at 10 A discharge current, and no cracking and porosity at 5.5 A discharge current (Figure 2). Coatings produced using the WC tool electrode resembled the coating produced using a TiC electrode, again exhibiting roughness, porosity and cracking in a cellular pattern.

Zr exhibited notably less cracking and porosity compared to WC and TiC. Cracking, when present, was typically distributed in a cellular pattern, consistent with the interface of individual discharge craters/deposits.

3.2 Multi-layer coating morphology

The single tool electrode coating data highlighted that crack and pore free surfaces could only be produced using Si tool electrodes. Hence, firstly here, coatings of sequentially processed TiC (Set A) and Si (Set B) layers were investigated, with a view to reducing the high levels of cracking and porosity associated with the EDC processed TiC coatings. Composite coatings were produced using increasing amounts of wear from the Si tool electrode onto TiC coatings produced using 0.5 mm of electrode wear (Table 2). Figure 2 presents SEM images of the surface morphologies of these composite coatings, whilst associated roughness (expressed through the *Sa* texture parameter) and crack density data are presented in Figure 4. For comparison, a double-layer coating from 0.5 mm of TiC(A) followed by 0.5 mm of TiC(B) is also shown, to prove the influence of using the Si electrode on coating morphology.

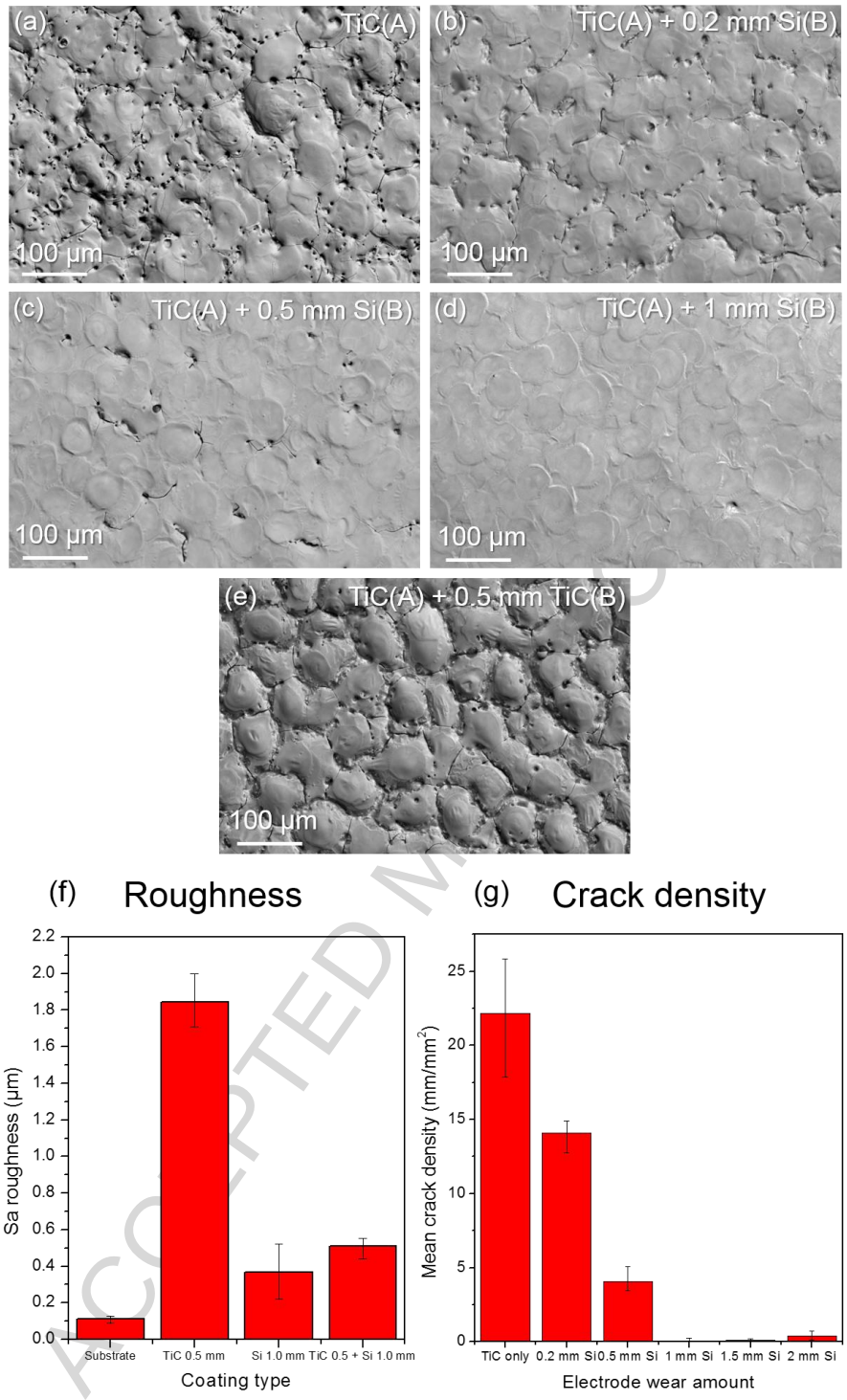

Figure 2 Morphology of TiC coatings surfaces after another coating of using an Si electrode (a)-(d), and (e) coating with a second layer of TiC, (f) reduced *Sa* roughness of Si and TiC/Si coatings compared to TiC only, and (g) effect of different amounts of silicon second coating on surface crack density. Error bars are the minimum and maximum of the values collected.

Based on SEM imaging, the majority of the negative surface properties associated with normal single layer TiC coating were eliminated by additional coating of silicon with 0.5 mm of electrode wear. Some cracking is still present but porosity is eliminated. To further optimise the phenomenon of surface crack reduction via the addition of an Si coating, increasing electrode wear amounts were investigated. Based on the initial result of significant crack reduction occurring after 0.5 mm coating of both TiC and Si, further tests were conducted using 0.2 mm, 1 mm, 1.5 mm and 2 mm silicon electrode wear amounts to establish if complete crack removal is possible. The change in surface crack density with increasing feed amount of the Si electrode on the TiC/Si combined coating is also shown in Figure 3 (g). The negative surface characteristics of the TiC coating were eliminated after 1 mm of wear from the silicon electrode. The surface topography is dominated by smooth overlapping craters and resembles the surface finish produced on a single coating of Si. After 0.2 mm of silicon coating, porosity and cracking remained prevalent on the surface, and after 0.5 mm, the smoother crater topography is dominant. In order to prove whether the final surface properties depend on the use of silicon as opposed to TiC, a multi-layer coating using a second layer of 0.5 mm of TiC but using the lower current parameter was made. This surface can be seen in Figure 2 (e). Despite the same electrical parameters, porosity and cracking dominate the surface, compared with the silicon surface in Figure 2 (c). *Sa* values of the polished substrate, a TiC coating, an Si coating and a TiC/Si combined coating were measured and are shown in Figure 2 (f).

The surface crack density of the TiC + 1 mm Si coating is reduced by a factor of approximately 500 in comparison with the simple TiC coating, with only small regions of occasional cracks remaining. Similar levels of cracking remain on the 1 mm, 1.5 mm and 2 mm samples. No further improvement was measured in the latter two samples. No porosity

was seen on the surface of the 1, 1.5 and 2 mm silicon coated surfaces. As shown in Figure 2 (f), roughness of the TiC + 1 mm Si sample is reduced from a mean of 1.85 µm *Sa* roughness of the TiC surface to 0.51 µm. The roughness of the Si only coated surface is 0.37 µm. The variation in roughness for each sample is also reduced for the double layer coating.

To help elucidate the balance between material removal and material deposition, topographical heights maps of a TiC, Si and a combined TiC/Si coating are shown in Figure 3 along with an optical micrograph of the same region (both obtained by measurement with the Alicona Infinite Focus G5 focus-variation microscope). A TiC coating was prepared first, then a Si coating was prepared on the edge of the TiC coating, to yield four distinct patches of coating as shown below.

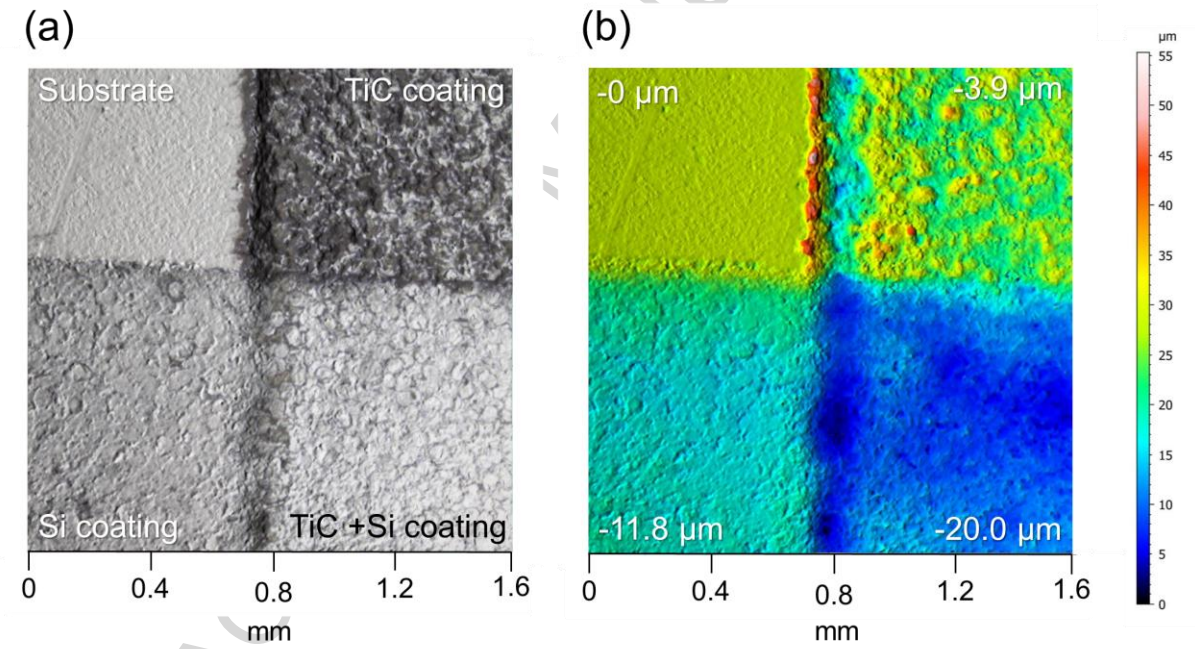

Figure 3 (a) Optical image and (b) topography height map of substrate, TiC (0.5 mm(A)), Si (0.5 mm(B)) and TiC (0.5mm (A)/Si (1 mm(B)) coatings, revealing extent of material removal during surface treatment

Height discrepancies between differently coated regions were assessed by averaging the height values of each region separately, using the substrate region as reference. Based on the

height map data shown in Figure 3, coating using either a TiC or Si sacrificial electrode results in net material removal. In the case of TiC (from 0.5 mm wear), a mean height difference of -3.9 µm was measured for 0.5 mm of electrode wear. However, it should be noted that many of the topographical peaks are above the height of the substrate, meaning it is likely that the coating process is in equilibrium with the material removal process. In the case of Si (0.5 mm wear), all regions of the coating were at a lower height than the substrate. For the TiC/Si coating, for which 1 mm of wear was used for the Si coating stage, the mean depth from substrate was -20 µm, greater than the simple addition of the two single layer coatings. This suggests that longer coating times yield great material removal in the case of Si electrodes and the coating/removal process is not in equilibrium.

Double-layer coatings were then prepared using combinations of TiC, WC and Si. Figure 4 shows SEM images of three examples of such coatings, in which morphologies characteristic of the case of the second material being deposited as a single layer are dominant. For example the TiC/WC coating resembles the WC simple coating, and the WC/TiC coating resembles the TiC coating. For Si/TiC, the TiC morphology is again dominant. In all such cases, the surfaces are characterised by the presence of cracking and porosity.

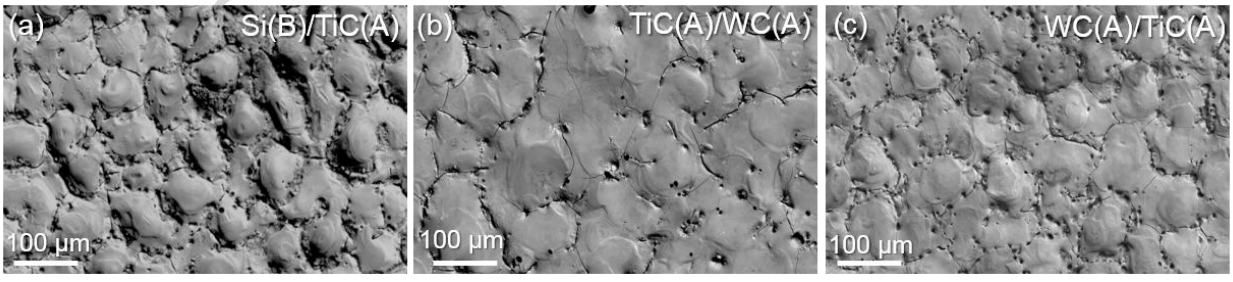

Figure 4 SEM images of double-layer coatings of (a) Si(B)/TiC(A), (b) TiC(A)/WC(A) and (c) WC(A)/TiC(A)

3.3 Coating composition

EDX data for the coatings produced using parameter Set A processing conditions are presented in Table 3, along with melting and boiling point values for the tool electrode materials. EDX analysis here was performed using a large area scan of 1 mm^2 of the surface of the coatings.

Table 3 Single layer EDX compositional data for the developed coatings (Parameter Set A). Remaining elemental composition for all samples is other constituents of steel.

Tool electrode	Melting point / °C	Boiling point / °C	Wt.% of main element, C and Fe
TiC	3065 [17]	4820 [18]	Ti 39.6, C 29.7, Fe 21.8
WC	2785 [19]	6000 [20]	W 40.5, C 27.7, Fe 21.3
Zr	1854 [21]	4406 [21]	Zr 9.5, Fe 44.7, C 20.2
Si	1410 [22]	2357 [23]	Si 9.8, Fe 52.5, C 16.6
Cu	1083 [22]	2562 [22]	Cu 1.1, Fe 48.8, C 28.5

Coatings produced using high melting point TiC and WC tool electrodes and Set A processing conditions contained much higher amounts of their primary elements, Ti and W, respectively, as compared to coatings produced using Si or Zr tool electrodes. Coatings produced using the lowest melting point Cu tool electrode retained the smallest amount of the primary element, at a level of 10% by weight of the Si and Zr. At the lower current parameter, the % of silicon by weight dropped to 5.4% based on an area EDX scan.

EDX surface data for the multi-layer coatings is shown in **Table 4**. Interestingly, despite yielding a similar surface morphology to the single layer Si coating, the TiC/Si coating

yielded only 1.9% Si with a significant level of Ti at 24.2% remaining. With the opposite multi-layer coating type: Si(B) followed by TiC(A), coated silicon was effectively eliminated as its weight % dropped to 0.2, a level present in the substrate material. The Ti level remained high, similar to that of a single layer coating, indicating that the TiC deposition is unaffected by a silicon coating beneath, whereas the ability of Si to yield a coating is notably affected by the presence of a TiC electrode beneath. WC as a single layer coating was seen to yield a heavily machined cavity despite the significant attachment of material. In the TiC/WC multi-layer coating this phenomenon is reflected given no Ti remained after coating and a composition of W reflecting that of a single layer coating remained.

Table 4 Multi-layer EDX compositional data

Tool electrode	Wt.% of main element, C and Fe
TiC(A) / Si(B)	Ti 24.2, Fe 31.9, C 27.3, Si 1.9
Si(B) / TiC(A)	Ti 41.7, C 29.3, Fe 20.5, Si 0.2
TiC(A) / TiC(B)	Ti 27.5, C 37.6, Fe 23.4
WC(A) / TiC(A)	Ti 29.3, C 28.0, Fe 18.1, W 17.5
TiC(A) / WC(B)	W 39.4, C 25.5, Fe 24.3,

3.4 Cross-sectional characterisation

Cross-sectional SEM/EDX analysis was performed to clarify the composition of single and multi-layer coatings, and elucidate mixing phenomena in such cases. Thickness of the coatings was also examined.

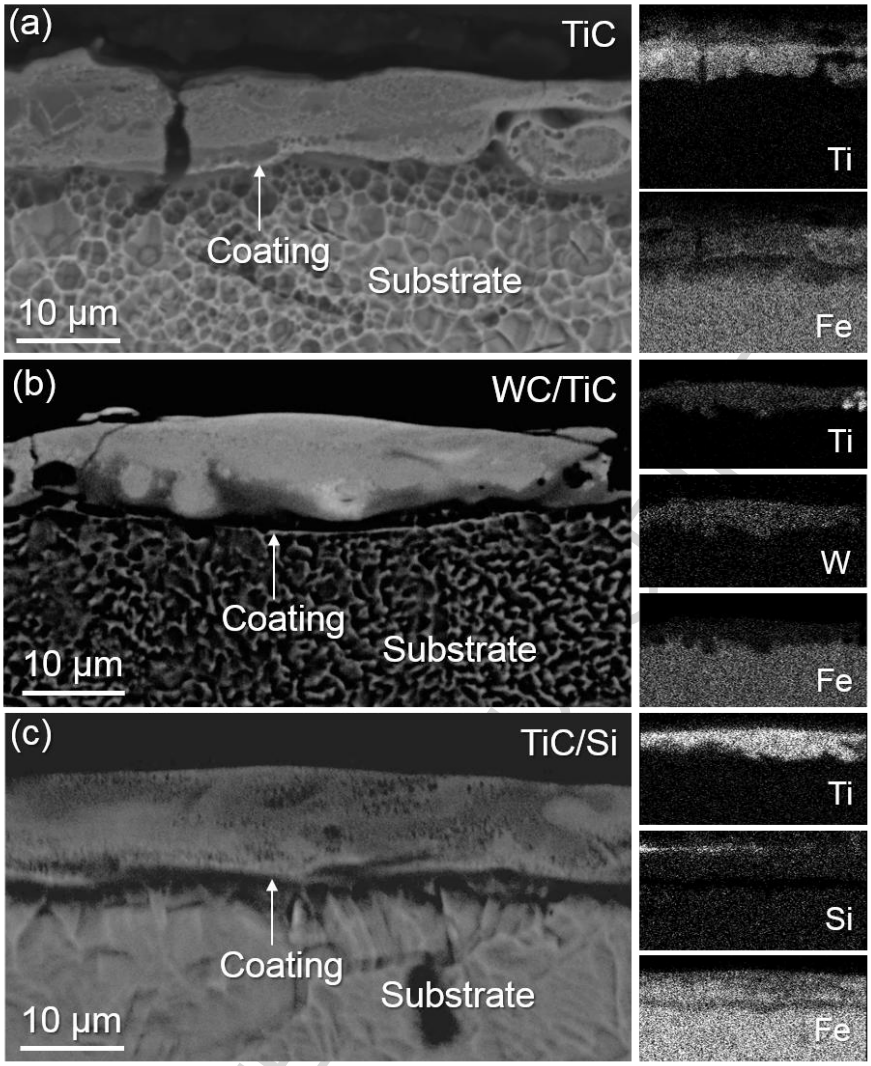

Figure 5 Cross-sectional SEM images of TiC(A), WC(A)/TiC(A) and TiC(A)/Si(B) coatings with EDX maps of primary elements. Significant intermixing can be seen in the WC/TiC coating.

The three coatings shown in Figure 5 - TiC, WC/TiC, and TiC/Si, all exhibited very similar thicknesses. This is expected given the same basic EDM parameters (current and on-time) were used for the deposition of all coatings, and it is well known that the recast layer in EDM, and therefore the coating thickness in EDC, depends primarily upon the current and on-time parameters [24, 25]. For the coating in Figure 5 (c), the Si was deposited using a lower current, and therefore the thickness of the TiC initial coating deposited with the higher current parameter takes precedent.

In previous work by the authors, it was observed that deposition of material via EDC by a single spark produces a deposit of a similar depth to the final coating [10]. Therefore the majority of the coating process involves re-melting of previously deposited material. Prior work also suggests that TiC coatings produced on a steel substrate by EDC are composite in nature, with TiC grain sizes as small as tens of nm, in a matrix of Fe. In the present work, the coatings in Figure 5 (a) and (c) contain mostly uniform distributions of Ti and Fe. In the case of the TiC/WC coating, the W and TiC are again uniformly distributed. Some pure TiC powder deposits can also be seen in Figure 5 (b). The uniform distribution of Ti and W is key to a successful composite coating and suggests that both materials are likely fully molten upon deposition by EDC. For the TiC/Si coating, Si was particularly concentrated at the top of the coating layer. Figure 6 shows more detailed images of cross-sections of the TiC and TiC/Si coatings.

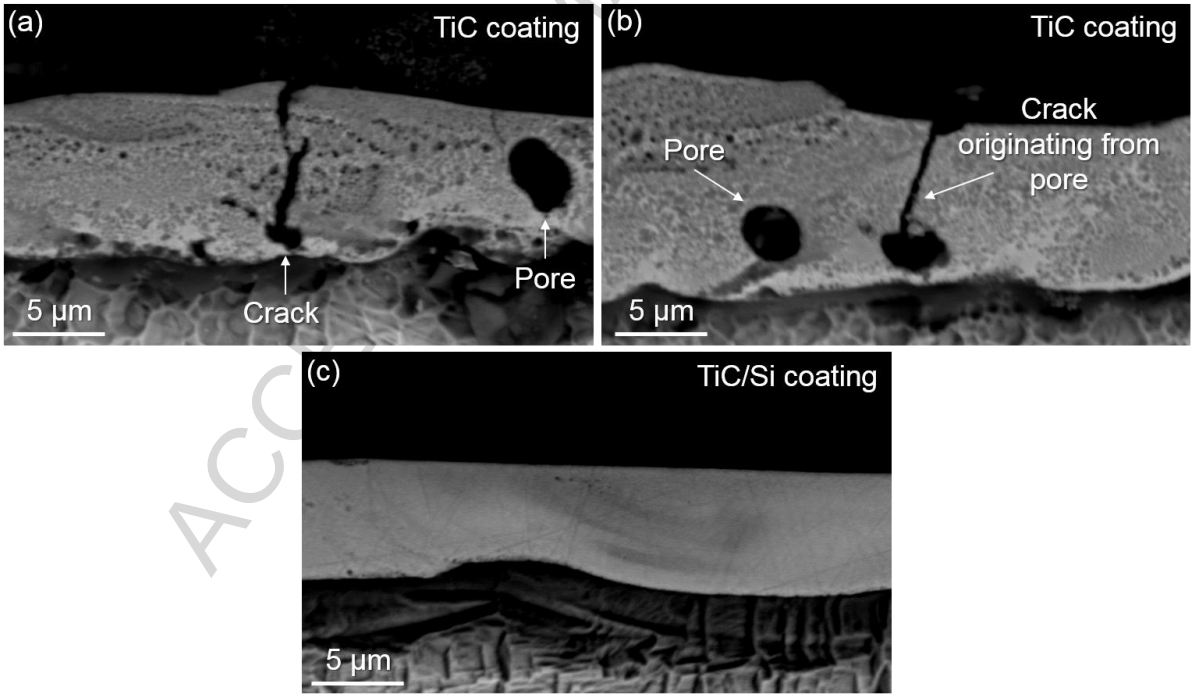

Figure 6 Back-scattered electron images of cross-sections of (a) and (b) TiC and (c) TiC/Si coating, revealing elimination of cracking and porosity

Extensive cross-sectional imaging was performed, and based on SEM imaging, porosity and cracking were observed to be entirely eliminated in the TiC/Si combined coatings. This can be contrasted with the examples of porosity which have diameters up to 50% of the thickness of the coating in the case of the TiC coatings, as well as cracking which penetrates the entire thickness of the coatings. Additionally, there was evidence that cracking in some cases originated at pores. In the authors' prior TEM work [10], sub-micron scale carbon deposits were observed within the TiC coating. In both the TiC and TiC/Si coatings, sub-micron scale dark (in BSE mode) regions can be seen, and these are thought to be carbon rich regions, as opposed to sub-micron scale porosity. EDX at this scale however is not accurate and the elimination of extremely fine porosity cannot be confirmed without multiple TEM samples.

3.5 Microstructure

To understand the microstructural composition of the single and double layer coatings, with particular emphasis on the crack/pore free TiC/Si coatings, X-ray diffraction was performed on the steel substrate, a single TiC coating, a TiC/Si double coating and the TiC electrode. All coatings were produced using 0.5 mm wear from electrodes. The results are shown in Figure 7.

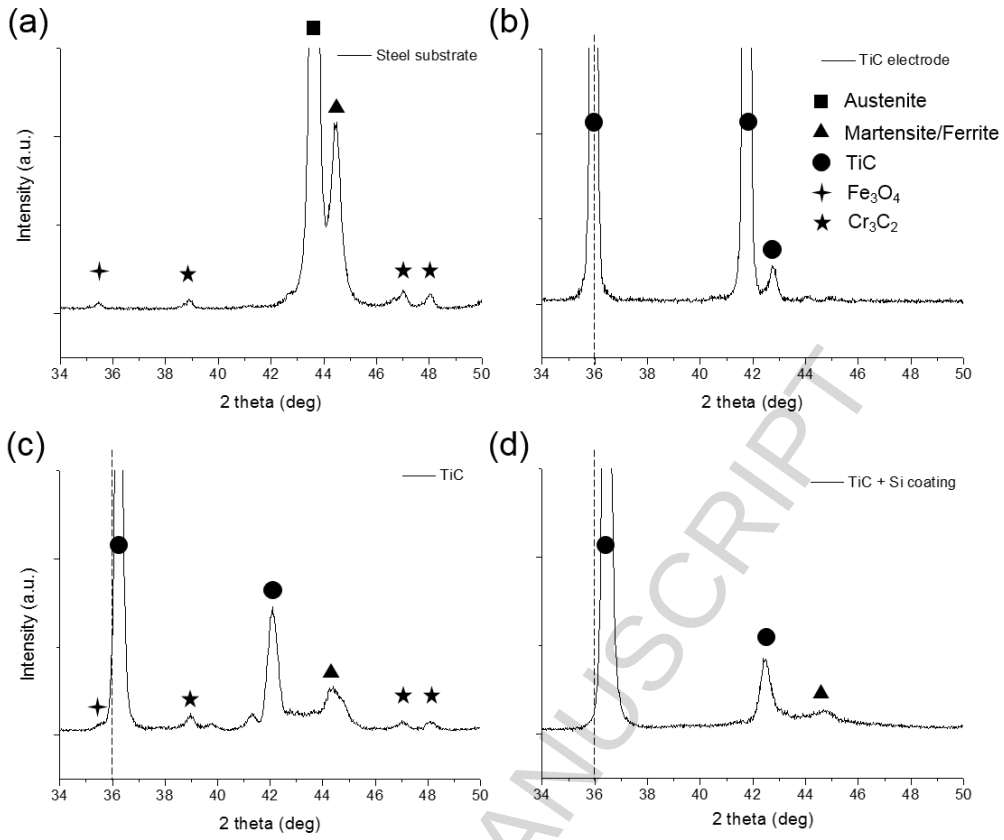

Figure 7 XRD diffractograms of (a) substrate, (b) TiC electrode material (c) TiC(A) coating and (d) TiC(A)/Si(B) coating

After the application of a single coating of TiC on the steel substrate, the dominant austenite phase from the steel was no longer observed. The martensite phase, however, was still detected in the coating layer, explained by rapid quenching assisting martensite formation, along with the dominant TiC phase. The TiC peaks present in the TiC coating are unchanged from the TiC phase present in the electrode material. After the application of a silicon coating to the TiC coating, the martensite peak is further suppressed. No silicon based phases were detected in the scan, likely explained by the low weight % of Si in the coating, beneath the measurement limit in the case of a small level of SiC being formed for example. This could also be explained by no single phase being formed in the coating, and phases present are split between pure Si and SiC for example, further reducing the ability of the phases to be measured. Although before and after the Si coating, the same TiC phase is present, there was

a notable shift to the right of all TiC peaks. A dotted line is shown for comparison to the position of the primary TiC peak in the electrode. The martensite peak however was not shifted, suggesting that the shift observed is not due to sample error but can be explained by the presence of strain in this phase. A significant change in the ratio of peak heights can be seen in the TiC coating compared to the electrode material, indicating the coating process is producing a preferential orientation effect on the TiC phase. This peak height ratio is further exaggerated after the addition of the layer of silicon.

3.6 Hardness

Nanoindentation was performed on the cross-sections of layers of Cu(A), TiC(A), as well as TiC(A)/Si(B) and WC(A)/TiC(A). Mechanical properties measured by nanoindentation are summarised in Table 5. Box plots of the hardness results for these coatings compared to the unaffected steel substrate are shown in Figure 8.

Table 5 Hardness and standard deviation measured by nanoindentation

	Steel	**Cu**	**TiC**	**TiC/Si**	**WC/TiC**
Mean hardness (GPa)	1.90	11.0	21.8	11.4	19.1
Standard deviation (GPa)	0.28	3.0	2.99	1.21	3.16

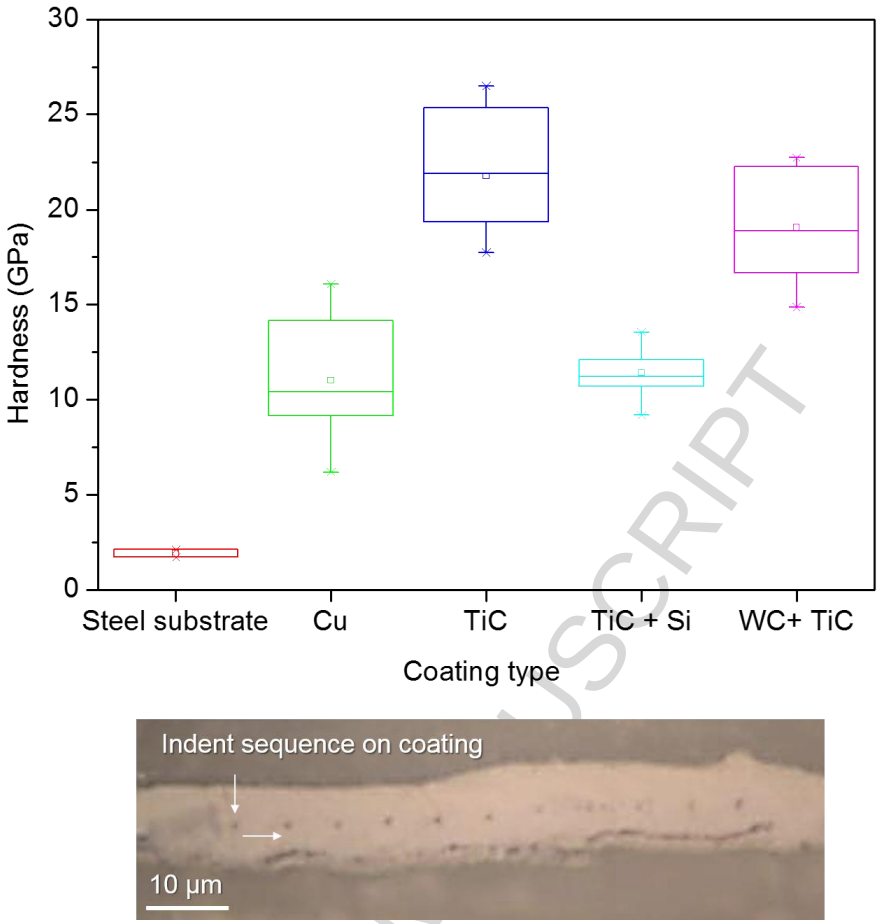

Figure 8 Box plots of hardness data from different coating types, compared to 304 stainless steel substrate. An optical image of the indents on the TiC coating are also shown.

It is clear that all layers produced using EDC exhibited much higher hardness compared to the steel substrate. The mean hardness of the EDM layer (Cu based coating) was approximately 6 times larger than the unaffected substrate material, at 11.0 compared to 1.9 GPa. This is despite the addition of 1.1% of the softer Cu to the recast layer. This is a key result as it indicates that the hardness of the coating is likely also to be strongly dependent on microstructural transformation and refinement as well as compositional changes. The single TiC coating yielded the highest mean, minimum and maximum hardness values from the four different coatings tested. The range of hardness measured for the TiC coating was between 25.6 and 17.7 GPa, with a mean of 21.8 GPa and standard deviation of 3.0 GPa. This can be

compared to the Cu coating which yielded a hardness range between 6.2 and 16.1 GPa, with a mean of 11.0 GPa, and a standard deviation also of 3.0 GPa. Therefore the highest individual hardness value measured on the Cu coating was close to the lowest value measured on the TiC coating. The TiC/WC combined coating yielded a mean hardness of 19.1 GPa, with a standard deviation of 3.16. The slightly reduced hardness of the combined coating can be explained by the lower hardness of raw WC compared to TiC – 15 compared to 30 GPa respectively. Previous TEM work on TiC coatings on steel indicates that the layer is a composite of an iron phase, likely martensite, and TiC. Because of this, the hardness of the TiC layer reflects an average of both the steel phase (itself hardened via martensite formation and inherently fine grain size) and the pure TiC. This rationale also explains the lower hardness of the TiC/WC phase.

The hardness results from the TiC/Si coating which produced a mean hardness much lower than the single TiC coating, but similar to the Cu coating, at 11.4 GPa, however with a much smaller standard deviation value – 1.21 GPa. Interestingly, despite only 5.4% Si detected on the surface on the coating, a significant and repeatable decrease in hardness was measured. The addition of silicon as a composite material to the workpiece therefore has a significant role in modifying the overall mechanical properties of the coating. To better represent the variation in hardness data, load-displacement curves from which hardness data was calculated are shown in Figure 9.

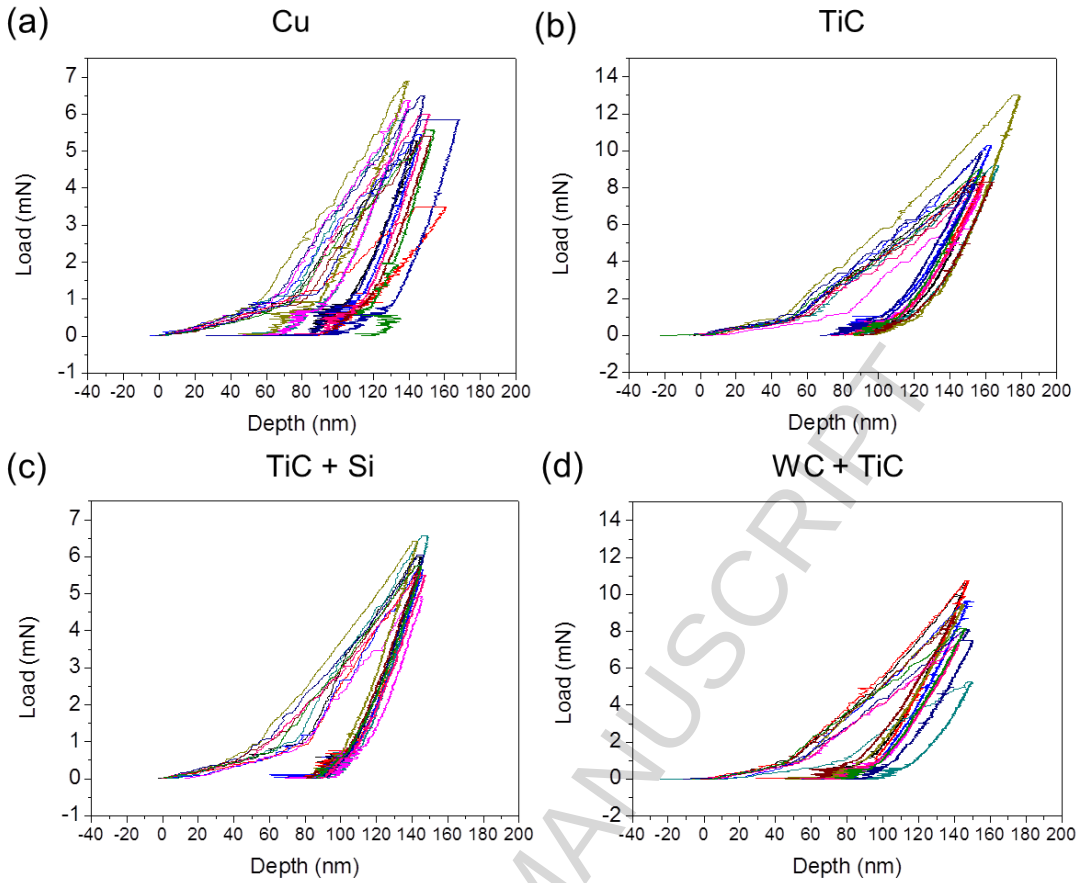

Figure 9 Load-displacement curves for Cu, TiC, TiC/Si and WC/TiC ED coatings. TiC curves show much greater consistency in both loading and unloading. This is represented by lower % variation in hardness values as shown in Figure 8. y-axis scales of the (a) and (c) are 50% of (b) and (d).

The load-displacement curves reveal data on the progress of the indentation with depth into the coating sample. It should be noted that the y-axis scales of the softer Cu and TiC/Si graphs are 50% of those of the TiC and WC/TiC.

When we consider the Cu coating, it appears that the data is the least repeatable of all samples. Specifically, the coating yielded two curves with significant flat-tops. The flat-top effect was not present in the other coating hysteresis data, suggesting the plastic deformation mechanics of these coatings are more uniform compared to the simple Cu coating. In the experimental section, it was explained that the indentation is held at maximum load for 20

seconds to allow for creep to occur before unloading. In two cases for the Cu based coating, an increase in depth of approximately 20 μm with no increase in load took place. This large variation in mechanical properties may be explained by indentation taking place in regions of concentration of the much softer Cu, inhomogeneities in material composition or coming in contact with porosity or cracks. Given the low level of Cu present in the coating produced using a Cu electrode, it is likely that the majority of the indents, which yielded hardness values of approximately 11 GPa took place in regions of only the recrystallized steel phase as this is consistent with the substrate material.

3.7 Deposit analysis

The composition of Si using the same coating parameters as the TiC is much lower than Ti in the TiC coating. To explain the difference in both morphology and amount of material adhesion which occurs during coating with TiC and Si, imaging and EDX analysis of individual discharge craters were performed. BSE images of TiC and Si craters produced using identical parameters and imaged at the same magnification, are shown in Figure 10 (a) (b) and (c). A Si crater at the lower current setting is shown in (d).

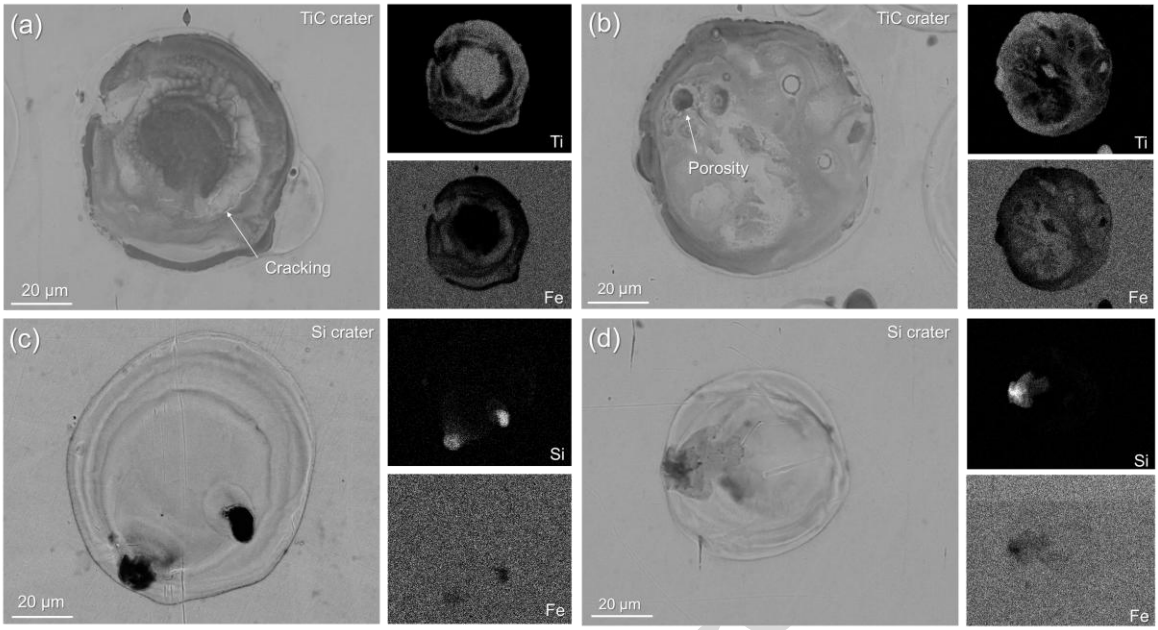

Figure 10 BSE images and EDX maps of craters produced using (a) and (b) TiC electrode at Parameter Set A revealing cracking and porosity respectively (c) Si electrode at Parameter Set A and (d) Si electrode at Parameter Set B

The craters imaged in Figure 10 were chosen as they were representative of those craters which contained deposited material for each electrode type. The clearest difference between craters is that the Ti is distributed across the majority of the TiC craters in Figure 10 (a) and (b), and is present up to the crater boundary. This can be contrasted with the Si crater, for which deposits of Si are present in only small regions. This phenomenon is typical for a large number of craters imaged. The amount of Si in the deposits in Figure 10 (c) is 43.0% and 61.5% for the left and right respectively, much higher levels than the final composition of Si coatings. In the centre of this Si crater, the amount of Si and C is 1.80% and 9.94% respectively, compared to 0.48% and 7.53% respectively from an unaffected region outside the crater. For the TiC crater, the amount of Ti and C in the centre of the crater is 74.56% and 23.47% respectively, with only 2.3% workpiece elements detected. For both Si and TiC coatings, the composition of coating elements is significantly lower than the localised regions analysed in the craters. In the TiC crater images, cracking as well as porosity were common,

as can be seen in Figure 10 (a) and (b). When using the Si electrode, the craters exhibited neither cracking nor porosity for both the high current and low current parameter. Craters also generally had a smoother morphology when the Si electrode was used, even in locations where significant deposition took place.

4 Discussion

4.1 Crack and pore elimination

On a 304 stainless steel workpiece, a coating with TiC as the dominant phase and dominant composition can be produced by EDC, containing a negligible number of cracks and level of porosity by the deposition of a second layer deposited from a pure silicon electrode. The thickness of coatings in EDC, as is the case for the recast layer in EDM, is independent of machining time. Therefore the reduction in crack and pore density with increasing Si electrode wear depth is not explained by the addition of an increasingly large Si layer on top of the TiC coating. Instead, with a longer coating time, the likelihood of sparking occurring in all regions of the surface increases, thereby increasing the likelihood of cracking and porosity to be eliminated.

To understand the absence of cracking in TiC/Si coatings, the single layer coatings should be considered. Based on the coating morphologies in Figure 1, it is clear that the silicon coating is uniquely characterised by an absence of cracks, compared with coatings created using TiC and Cu electrodes under identical conditions. When TiC/Si coatings were produced, cracking was still absent, despite the relative dominance of the TiC phase. Considering the similar sizes of the TiC and Si craters under the same electrical conditions, it is likely that the energy of each spark which reaches the surface of the workpiece is not notably affected by the influence of silicon particles on the discharge process. A smaller discharge crater would be

consistent with reduced discharge energy [26]. To explain the phenomenon of vastly different crater morphologies dependent on electrode material, we can consider phenomena associated with powder addition to EDM machining. It is well known that powder addition to the discharge gap can significantly modify discharge crater morphology. Addition of silicon powder to the EDM has been shown to yield an improved surface finish compared to a clean discharge gap [27]. In the case of silicon powder, this effect has been shown to yield a surface roughness reduction of 80% compared to the use of manganese powder which yielded only a 50% reduction [28]. Additionally, in the latter work, the recast layer produced was absent of pores and cracks in the case of use of silicon powder, as opposed to a recast layer still characterised by some level of pores and cracks in the case of manganese powder, under identical parameters. The explanation given for why silicon yielded an improved recast layer was the threefold lower density of silicon compared to manganese, and hence it will be more buoyant and therefore more uniformly distributed in the dielectric, thereby promoting more uniform discharges and therefore a more uniform recast layer. However, this explanation is overly simplistic and does not consider the effect on fundamental discharge properties. Uno et al. performed fundamental EDM testing using addition of Si powder to a kerosene EDM fluid [29]. Normal machining, as well as single crater analysis was performed. Single craters produced using Si powder addition were significantly less undulating than the normal EDM craters under identical conditions, despite overall recast layer size being similar. Impact force of a single electrical discharge on the substrate was measured using a piezoelectric dynamometer. The maximum value of the impact force in the case of the clean EDM oil was two times higher than that of the silicon powder mixed oil. This was explained by an increased inter-electrode gap distance at the time of discharge from 17 to 92 μm in the case of clean and silicon mixed oil respectively. Such an increased gap distance was used to explain the reduction in impact force and hence smoother craters. Given the reduced impact force

associated with increase discharge gap, and reduced material ejection thought to occur under reduced impact force, this may explain the reduced porosity which is also noted on craters and layers made using an Si electrode alone. Porosity is thought to occur due to gas trapped during the discharge process, and hence a lesser effect of the discharge on material melting and ejection would likely reduce the prevalence of porosity within each crater. A more violent material expulsion and hence resolidification mechanism may also explain reduced crack density associated with larger discharge gaps. Interestingly, Uno et al. [29] measured a delay in the onset of maximum impact force in the case of silicon powder mixed EDM, by several µs, although this was not discussed in the paper. Considering the discharge on-time was only 8 µs in the present work, this delay may play a significant role in crater formation. Uno et al. [29], despite showing that discharge impact force is correlated with improved crater smoothness, did not explain the mechanism by which reduced impact force occurs in the case of larger discharge gaps. More recent fundamental work in EDM has revealed that bubble formation and expansion during and after discharge plays a critical role in the material removal mechanism [1, 30, 31]. Most relevantly, Zhang et al. [32] have shown that bubble expansion velocity and pressure are highest for small gap widths, and this is correlated with impact force on electrode. It should be noted that the exact melting and material ejection mechanisms in EDM complicated and remain contentious, however it is well understood that gap width plays a key role in discharge crater properties and hence final surface properties.

When the single discharges are considered in Figure 10, smooth craters can be seen in the case of the Si electrode, despite the similar diameter when compared with the crater associated with the TiC electrode under identical conditions. Given the similar crater size, this implies overall energy supplied is thought to be similar in both cases, thereby giving evidence that impact force plays the primary role in the differing crater morphologies, and

hence overall coating morphology in the case of pure Si and TiC/Si coatings. To explain the difference in gap width and hence crater morphology for TiC and Si sacrificial electrodes, lower density and hence higher buoyancy of Si in comparison TiC means a higher uniformity of polarisable electrically conductive particles assist in dielectric breakdown, thereby increasing gap width [28]. To summarise the mechanisms which result in improved layer properties in TiC/Si based composite coatings, a schematic is shown in Figure 11.

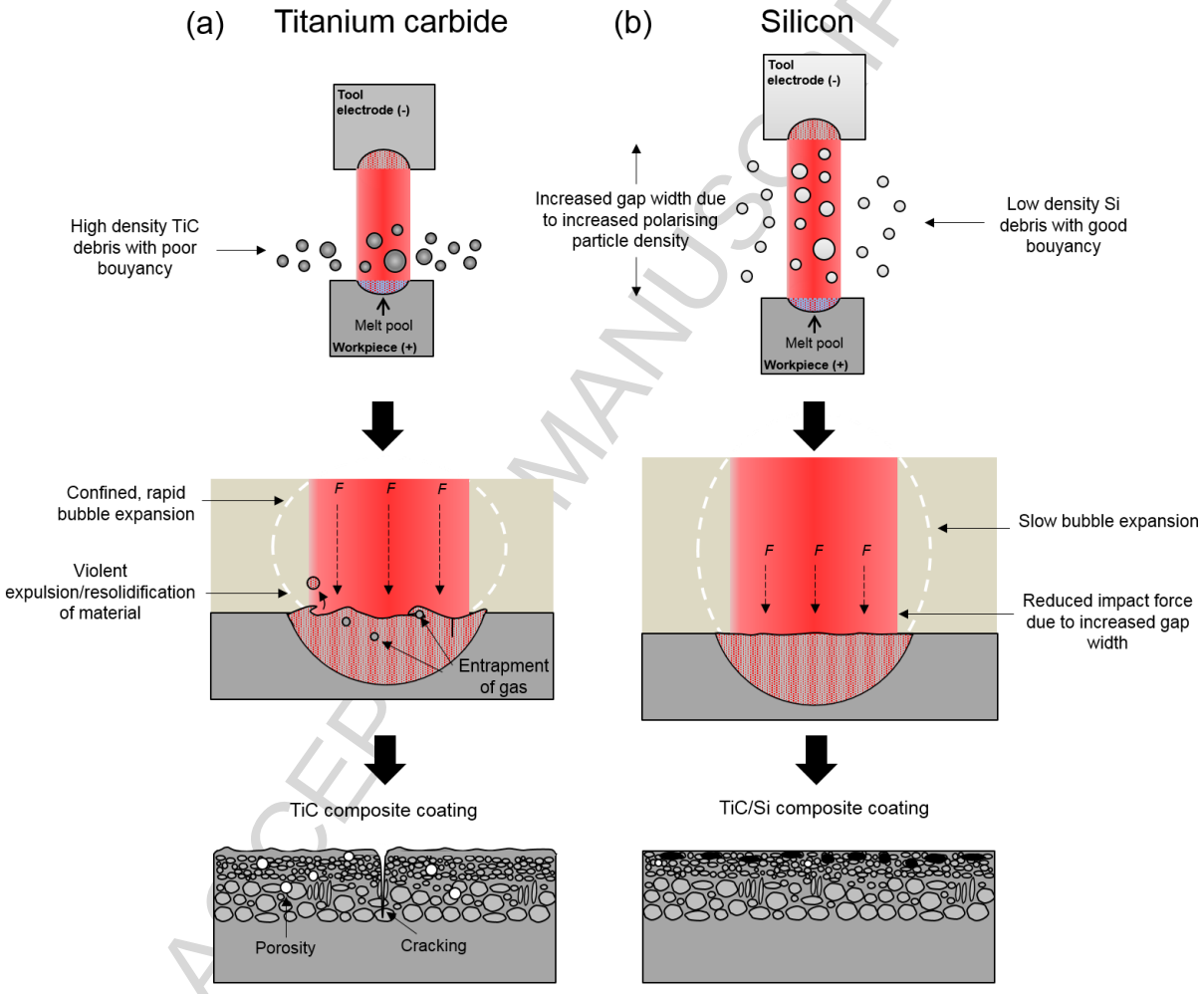

Figure 11 Schematic showing mechanism of improved layer properties when silicon is used as sacrificial electrode at final coating stage. Lower density Si results in increased gap width due to more uniform and higher density distribution of particles in the discharge gap. As a result, bubble expansion is slower than in the case of a smaller gap.

Expulsion and resolidification of material is less violent, thereby resulting in a composite layer with fewer pores and cracks and lower surface roughness.

It can be noted Uno et al. [29] showed that carbide precipitation exacerbated crack generation in the recast layer via the differential in thermal expansion between carbide and surrounding metal. Therefore with the inherently larger overall level of movement and resolidification of TiC in the coating layer in the case of TiC work, this would also explain the higher level of cracking in the TiC based coatings. In single discharge analysis, in the case of craters formed using the Si electrode, cracking was not seen in the location of Si deposits. However, it is clear that in the combined TiC/Si coating, the weight % of Si is low compared to the dominant TiC composition within the layer. Despite this, on the surface and in cross-section, the composite TiC/Si coating has a structure with cracks virtually eliminated. This indicates that the effect of less violent expulsion and resolidification mechanisms as a result of increased gap widths in the case of an Si electrode, therefore likely plays the more significant role in crack density reduction.

4.2 Composition and material transfer

Considering the EDX results of the combined coatings in Table 4 as well as the XRD data in Figure 7, the TiC/Si coating can be considered a composite dominated by TiC. From the perspective of exploiting the coating for its mechanical properties, for example wear, the preservation of the TiC phase is critical. In Table 3, the EDX results of single layer coatings using identical parameters but with different electrode materials are shown. The two carbide materials: TiC and WC, yielded a coating which was dominated by the coating elements, whereas zirconium, silicon and copper all yielded a much lower %. Considering the strong correlation between melting point and weight % of the primary element of the electrode adhered to the coating, it is likely that the much higher melting points of the carbide materials

are the cause of a greater level of adhesion by coating. To understand the mechanism of coating in EDC, it should be considered in the context of the mechanism of electrical discharge processes. The basic principle of EDM is to remove material via melting and/or evaporation of the workpiece material via each discharge. In EDM, much of the molten material is ejected at the end of discharge duration, when a pressure drop occurs upon extinguishing of the plasma. Material is also thought to be ejected during discharge through boiling of the material heated by the plasma [31]. It is therefore expected that the melting point of a coated material will significantly affect the amount of material removed, and the amount left on the surface, by the inevitable material removal caused by discharge. In coating, it is desirable for this effect to be inhibited to prevent coating mass loss. In the case of TiC, due to its high melting point, material returns to the solid state more rapidly during discharge than silicon, resulting in a lower amount of remaining liquid upon the end of discharge. At the end of discharge, a pressure drop occurs which ejects remaining liquid material from the discharge crater, an effect which is inhibited by the presence of solid TiC. This may explain the lower remaining composition of Si in the discharge crater and therefore also in the final coating compared to TiC. In the authors' prior work [10], the microstructure of TiC based ED coatings was shown to consist of re-crystallised TiC but also contained entire particles thought to deposit directly and remaining un-melted. Therefore the extent of material survival and hence attachment clearly depends on the ability of the material to not melt and/or evaporate due to contact with the discharge plasma. A schematic is shown in Figure 12 which explains the mechanism by which materials with vastly different melting points show very different levels of attachment after discharge.

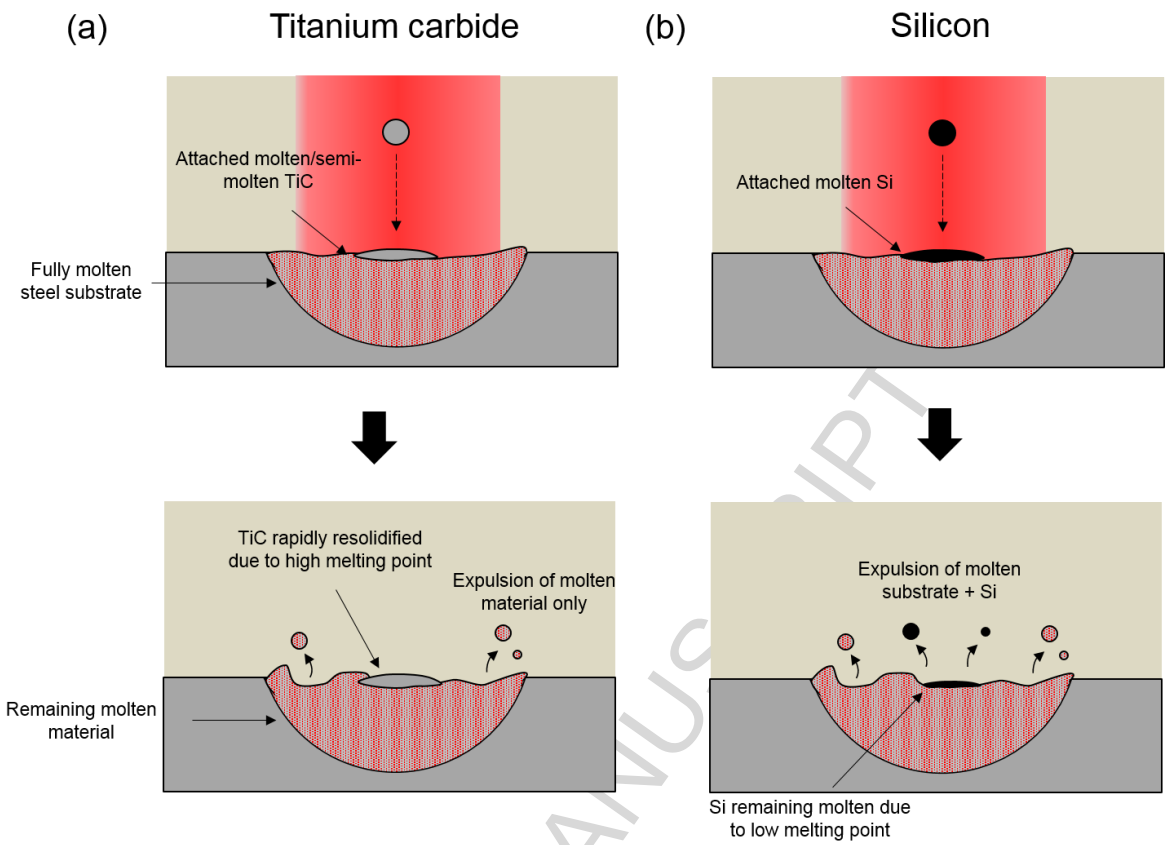

Figure 12 Proposed mechanism for enhanced material transfer in the case of higher melting point sacrificial electrode materials onto a steel substrate. TiC is thought to attach to the melt pool in the molten or semi-molten state, but upon discharge end, reaches its melting point and hence solidifies rapidly, leaving remaining molten substrate material (in the case of steel) to be preferentially ejected. In the case of Si attachment, its melting point is close to that of the steel substrate, and hence deposits remain molten with the steel and are expelled to similar extents.

In the schematic in Figure 12, initially during discharge on-time material movement into the melt pool is not different for each material type. However, upon discharge end and solidification, the high melting point TiC reaches its solidification point rapidly, thereby resisting material ejection. It should be noted that this model is relevant in the case of the substrate or coating with an overall melting point on the scale of steel.

In the XRD analysis shown in Figure 7, after a single TiC coating, and TiC/Si coating, the dominant phase is TiC which is unchanged from the TiC electrode. The ratio of TiC peak heights in the coatings however is changed compared to the peak heights of the TiC electrode with randomly oriented grains. This ratio is further altered after the Si coating. Since, according to XRD data, the same TiC phase is present and no new TiC based phases were detected in the coating compared to the original electrode material, this suggests that much of the TiC deposited may have stayed in the solid or semi-solid phase. The preferential orientation of grains indicated by the altered peak height ratios, and observed directly in cross-section [10], could be explained either by unidirectional grain growth upon cooling, or by stress induced deformation of grains. The specific reason for which cannot be explained without further high resolution microscopy. The absence of other phases in the coating however adds weight to the theory that insufficient melting of the TiC phase occurred to allow dissolution and a chemical reaction to take place. The microstructural composition of workpiece elements and Si therefore require more detailed analysis techniques including TEM to determine their exact form.

4.3 Hardness

This work expands on the fundamental understanding of EDC coatings via the mechanical and chemical characterisation of single and multi-layer coatings. Based on cross-sectional data in this study, it is evident that ED coating can produce on average a hard layer via the incorporation of TiC into the workpiece surface of steel, in a composite structure combined with a rapidly re-crystallised and hardened steel phase. The results clearly indicate that hardness is not consistent throughout the layer, but depends on location of indentation. For practical applications, including wear of the coating, local variation in hardness properties may not affect the overall performance as opposed to the mean hardness values.

The results in this work can be compared to a composite coating system created by pulsed laser melting of TiC on 304 steel [33]. In this study, a similar but thicker coating was produced (100 – 400 μm). By a similar mechanism to ED coating, the coating is formed by intermixing of TiC and steel via Marangoni convection, resulting in a composite final structure. Interestingly, the highest single hardness value measured in the TiC composite coatings by laser melting was close to the lowest value measured in the equivalent coating produced by EDC in the present study – approximately 18 GPa (~1800 HV). Under the laser conditions which produce this value (1 kW), the range of values was also highest, ranging from 1800 to 300 GPa, with mean hardness between 800 and 1100 HV. With higher laser powers, the variation in values is notably reduced, and the mean is reduced to ~500 HV and ~400 HV for 2 and 3 kW respectively. This suggests with greater intermixing of steel and TiC, the hardness is significantly reduced, towards the hardness of the bulk material. However in the case of EDC the hardness of TiC coatings remains significantly higher than the bulk material despite a notable standard deviation of hardness values.

Prior research on the mechanical properties of ED coatings has employed simple Vickers testing to determine the hardness of typical coatings produced by the process. In the present study, a more thorough examination of the mechanical properties of such layers was conducted via the nanoindentation process. The advantage of such a technique is the visualisation of the indents themselves to confirm the accuracy and distribution of indentation, and the inspection of the load-displacement data produced by the indentation technique to further scrutinise the testing process. In this study it was shown that the hardness of the EDC layer produced using a sacrificial TiC electrode is consistently harder than the layer produced via a Cu sacrificial electrode, which represents a simple EDM recast layer.

Despite these measurements, a significant variation in hardness exists across all layers tested by nanoindentation. Specifically, there was a standard deviation between 11% and 27% of the mean value. For example, the layer produced using a Cu electrode yielded a 2.99 GPa standard deviation value for a mean hardness of 11.0 GPa. The resulting highest hardness value measured on this layer was only just less than the lowest hardness measured in the TiC layer. The WC/TiC coating yielded a slightly reduced mean and range of hardness values, explained by the slightly lower hardness of pure WC compared to TiC.

To understand such a large variation in hardness results produced by nanoindentation, and the relationship between hardness and indent location, the size of indents should be considered based on the understanding of the microstructure and composition of the coating. It has been shown that the TiC coating structure has a graded size and distribution of TiC grains in an iron-based matrix [10]. The maximum depth reached in the indentation was 150 nm, therefore the largest width of material interrogated by the indent is 1.5 µm based on standard indent 1:10 depth:width aspect ratios. Therefore the majority of material subject to deformation is in the sub-micron scale. The indents on the TiC coating cross-section were at an average of approximately 4 µm depth from the top surface. When considering the structures presented in the cross-sectional TEM work, at 4 µm depth, TiC grains are separated by regions of steel matrix with distances of 100s of nm. Therefore it is reasonable that initial indentation on sections of the softer steel matrix could explain the lower bound of the hardness results for all coating samples. Similarly, it is clear than any indentation on a TiC based coating will at some point interact with both phases, and therefore the fact that the upper bound of hardness is lower than the theoretical hardness of TiC is explained by this.

The TiC/Si coating yielded a mean hardness value similar to that of the Cu based layer. This is despite the TiC content forming the majority of the coating in terms of composition, and Si contributing only 5-6% by weight maximum to the coating. It can be noted that SiC was not

detected by XRD analysis, which is expected to have a similar hardness to TiC, hence its absence would help explain the significant in reduction in hardness compared to the TiC coating. In the case of Si being present in the amorphous form, nanoindentation has measured its hardness at a mean of ~9.5 GPa [34]. Crystalline silicon nano-indentation hardness has been measured between 6 and 14 GPa, depending on orientation [35]. Hence a modest level of Si present possessing this range of hardness values could explain the significantly reduced mean cross-sectional hardness. The much reduced scatter of hardness data for the TiC/Si coating can also be explained by the reduced porosity present in the layer, giving further evidence that porosity is likely playing a role in the nanoindentation behaviour. Additionally, the contribution of residual stress to the load bearing behaviour cannot be ruled out and the residual stress condition of the layer should be considered for further work.

5. Conclusions

Next-generation recast layers on components machined by EDM will likely exploit EDC phenomena to yield a layer with favourable properties, in order to avoid recast layer removal. This work builds towards this goal by demonstrating a TiC based coating can be created without defects via the use of sequential Si coating. The main conclusions of the work are the following:

- A TiC based coating can be created absent of surface cracking and porosity on a stainless steel substrate by the re-melting of the layer with a second coating using an Si electrode with 1 mm of sacrificial electrode wear. In addition, no evidence of cracking and porosity was seen in cross-sectional analysis.
- In the case of Si particles in the discharge gap, enlarged discharge gap width, theorised to result in reduced impact force due to bubble expansion, explained the reduced cracking and porosity associated with Si based discharge craters and hence

coating properties. Similar sizes of Si and TiC individual discharges indicates that overall energy density is not notably affected. The lower density of Si compared to TiC, with therefore greater uniformity of particles in the discharge gap, lowering the dielectric breakdown strength and thereby increasing gap width, explains the improved properties of Si based coatings over those from TiC.

- A composite ceramic coating comprised of WC and TiC was fabricated using sequential coating of the former followed by the latter. The final layer comprised a highly uniform mix of both material types. This indicates EDC can be used for the fabrication of more complicated composite layers.
- The ability of EDC to transfer material from workpiece to substrate appears to depend strongly on thermal properties of the electrode material, specifically melting point. WC and TiC can be deposited and form the majority of the composition of the coating, whereas Cu and Si comprise a much lower level - ~2 and ~5.5% respectively. This is explained by the ability of material to resolidify quickly and thereby resist molten ejection and/or evaporation.
- Nanoindentation data showed that the TiC and WC/TiC coatings yielded the highest mean hardness values, both with a similar range of data. The WC/TiC coating yielded a slightly lower mean hardness of 19.1 compared to 21.8 GPa for the TiC, owing to the lower hardness of pure WC. A small level of Si (~5-6% at maximum) present in the TiC coating served to reduce the mean hardness of the coating notably, however the scatter in the hardness data was also reduced significantly owing to more uniform properties and morphology. Hardness of the ceramic based coatings was approximately twice that of the Cu machined layer under identical conditions.

Acknowledgements

J.W. Murray and A.T. Clare would like to acknowledge funding from EPSRC grant number EP/L017547/1. N. Senin wishes to acknowledge the grant: METROSURF (FP7-PEOPLE-IEF 624770) from the EC.

Data Availability

The raw/processed data required to reproduce these findings cannot be shared at this time as the data also forms part of an ongoing study

References

[1] M. Kunieda, B. Lauwers, K.P. Rajurkar, B.M. Schumacher, Advancing EDM through fundamental insight into the process, CIRP Annals - Manufacturing Technology 54(2) (2005) 599-622.
[2] T. Moro, N. Mohri, H. Otsubo, A. Goto, N. Saito, Study on the surface modification system with electrical discharge machine in the practical usage, Journal of Materials Processing Technology 149(1–3) (2004) 65-70.
[3] Y.-L. Hwang, C.-L. Kuo, S.-F. Hwang, The coating of TiC layer on the surface of nickel by electric discharge coating (EDC) with a multi-layer electrode, Journal of Materials Processing Technology 210(4) (2010) 642-652.
[4] P. Janmanee, A. Muttamara, Surface modification of tungsten carbide by electrical discharge coating (EDC) using a titanium powder suspension, Applied Surface Science (0) (2012).
[5] T.C. Lu, J. Yang, Z. Suo, A.G. Evans, R. Hecht, R. Mehrabian, Matrix cracking in intermetallic composites caused by thermal expansion mismatch, Acta Metallurgica et Materialia 39(8) (1991) 1883-1890.
[6] A. Simchi, H. Danninger, Effects of porosity on delamination wear behaviour of sintered plain iron, Powder Metallurgy 47(1) (2004) 73-80.
[7] L. Zhang, X.-h. Qu, B.-h. Duan, X.-b. He, M.-l. Qin, Effect of porosity on wear resistance of SiCp/Cu composites prepared by pressureless infiltration, Transactions of Nonferrous Metals Society of China 18(5) (2008) 1076-1082.
[8] J. Aktaa, K. Sfar, D. Munz, Assessment of TBC systems failure mechanisms using a fracture mechanics approach, Acta Materialia 53(16) (2005) 4399-4413.
[9] H. Chai, J. Fox, On delamination growth from channel cracks in thin-film coatings, International Journal of Solids and Structures 49(22) (2012) 3142-3147.
[10] J.W. Murray, S.J. Algodi, M.W. Fay, P.D. Brown, A.T. Clare, Formation mechanism of electrical discharge TiC-Fe composite coatings, Journal of Materials Processing Technology 243 (2017) 143-151.
[11] R. Tyagi, A.K. Das, A. Mandal, Electrical discharge coating using WS2 and Cu powder mixture for solid lubrication and enhanced tribological performance, Tribology International 120 (2018) 80-92.
[12] Z.-y. Zeng, H.-q. Xiao, X.-h. Jie, Y.-m. Zhang, Friction and wear behaviors of TiCN coating based on electrical discharge coating, Transactions of Nonferrous Metals Society of China 25(11) (2015) 3716-3722.
[13] S.J. Algodi, J.W. Murray, P.D. Brown, A.T. Clare, Wear performance of TiC/Fe cermet electrical discharge coatings, Wear 402-403 (2018) 109-123.

[14] N. Sumi, C. Kato, K. Shimada, T. Yuzawa, H. Teramoto, a. Mizutani, T. Kuriyagawa, Mechanism of Defect Generation in the TiC Layer and Si Layer by Electrical Discharge Coating, Procedia CIRP 42 (2016) 221-225.
[15] S.J. Algodi, J.W. Murray, M.W. Fay, A.T. Clare, P.D. Brown, Electrical discharge coating of nanostructured TiC-Fe cermets on 304 stainless steel, Surface and Coatings Technology 307 (2016) 639-649.
[16] D.A. Lucca, K. Herrmann, M.J. Klopfstein, Nanoindentation: Measuring methods and applications, CIRP Annals 59(2) (2010) 803-819.
[17] M. Bauccio, ASM engineered materials reference book, 2nd ed ed., ASM International1994.
[18] D.L. Perry, S.L. Phillips, Handbook of Inorganic Compounds, Taylor & Francis1995.
[19] D.R. Lide, CRC Handbook of Chemistry and Physics. 81st Edition E, Journal of the American Chemical Society 122(50) (2000) 12614-12614.
[20] R.C. Weast, D.R. Lide, U.o.R.I.C.R. Center, CRC handbook of chemistry and physics, (1978).
[21] W.M. Haynes, CRC Handbook of Chemistry and Physics, 95th Edition, CRC Press2014.
[22] M.J.O. O'Neil, P.E. Heckelman, C.B. Koch, The Merck Index: An Encyclopedia of Chemicals, Drugs, and Biologicals, 14th ed., Journal of the American Chemical Society 129(7) (2007) 2197-2197.
[23] R.J. Lewis, Hawley's Condensed Chemical Dictionary, 15th edition, Journal of the American Chemical Society 129(16) (2007) 5296-5296.
[24] J. Murray, D. Zdebski, A.T. Clare, Workpiece debris deposition on tool electrodes and secondary discharge phenomena in micro-EDM, Journal of Materials Processing Technology 212(7) (2012) 1537-1547.
[25] J.W. Murray, A.T. Clare, Repair of EDM induced surface cracks by pulsed electron beam irradiation, Journal of Materials Processing Technology 212(12) (2012) 2642-2651.
[26] B. Shao, K.P. Rajurkar, Modelling of the Crater Formation in Micro-EDM, Procedia CIRP 33 (2015) 376-381.
[27] H.K. Kansal, S. Singh, P. Kumar, Parametric optimization of powder mixed electrical discharge machining by response surface methodology, Journal of Materials Processing Technology 169(3) (2005) 427-436.
[28] A. Molinetti, F.L. Amorim, P.C. Soares, T. Czelusniak, Surface modification of AISI H13 tool steel with silicon or manganese powders mixed to the dielectric in electrical discharge machining process, The International Journal of Advanced Manufacturing Technology 83(5) (2016) 1057-1068.
[29] Y. Uno, A. Okada, Surface generation mechanism in electrical discharge machining with silicon powder mixed fluid, International Journal of Electro Machining 2(2) (1997) 13-18.
[30] J. Tao, J. Ni, A.J. Shih, Modeling of the Anode Crater Formation in Electrical Discharge Machining, Journal of Manufacturing Science and Engineering 134(1) (2012) 011002-011002-11.
[31] X. Yang, J. Guo, X. Chen, M. Kunieda, Molecular dynamics simulation of the material removal mechanism in micro-EDM, Precision Engineering 35(1) (2010) 51-57.
[32] Y. Zhang, Y. Liu, R. Ji, C. Zheng, Y. Shen, X. Wang, Transient dynamics simulation of the electrical discharge-generated bubble in sinking EDM, The International Journal of Advanced Manufacturing Technology 68(5) (2013) 1707-1715.
[33] C.K. Sahoo, M. Masanta, Effect of pulse laser parameters on TiC reinforced AISI 304 stainless steel composite coating by laser surface engineering process, Optics and Lasers in Engineering 67 (2015) 36-48.
[34] P. Danesh, B. Pantchev, J. Wiezorek, B. Schmidt, D. Grambole, Effect of hydrogen on hardness of amorphous silicon, Applied Physics A 102(1) (2011) 131-135.
[35] R. Hull, INSPEC, Properties of Crystalline Silicon, INSPEC, the Institution of Electrical Engineers 1999.

Table 1 Experimental parameters

Tool electrode materials	TiC, Si, Cu, WC, Zr
Workpiece material	304 stainless steel
Oil (dielectric)	Shell Paraol 250
Tool electrode polarity	Negative
Parameter Set A	320 V; 10 A current: 8 µs ON / 256 µs OFF
Parameter Set B	260 V; 5.5 A current: 8 µs ON / 64 µs OFF

Table 2 Coatings and parameter sets evaluated within this study

Electrode	Parameter Sets	Electrode wear (mm)
TiC, Si, Cu, WC, Zr	A	0.5
TiC, Si, Cu, WC, Zr	B	0.5
WC/TiC, TiC/WC	A / A	0.5 / 0.5
Si/TiC	B / A	0.2, 0.5, 1.0, 1.5 & 2.0 / 0.5
TiC/TiC	B / A	0.5 / 0.5
Si/TiC	B / A	0.5 / 0.5
TiC	A	Single discharge
Si	A	Single discharge
Si	B	Single discharge

Table 3 Single layer EDX compositional data for the developed coatings (Parameter Set A).

Remaining elemental composition for all samples is other constituents of steel.

Tool electrode	Melting point / °C	Boiling point / °C	Wt.% of main element, C and Fe
TiC	3065 [17]	4820 [18]	Ti 39.6, C 29.7, Fe 21.8
WC	2785 [19]	6000 [20]	W 40.5, C 27.7, Fe 21.3
Zr	1854 [21]	4406 [21]	Zr 9.5, Fe 44.7, C 20.2
Si	1410 [22]	2357 [23]	Si 9.8, Fe 52.5, C 16.6
Cu	1083 [22]	2562 [22]	Cu 1.1, Fe 48.8, C 28.5

Table 4 Multi-layer EDX compositional data

Tool electrode	Wt.% of main element, C and Fe
TiC(A) / Si(B)	Ti 24.2, Fe 31.9, C 27.3, Si 1.9
Si(B) / TiC(A)	Ti 41.7, C 29.3, Fe 20.5, Si 0.2
TiC(A) / TiC(B)	Ti 27.5, C 37.6, Fe 23.4
WC(A) / TiC(A)	Ti 29.3, C 28.0, Fe 18.1, W 17.5
TiC(A) / WC(B)	W 39.4, C 25.5, Fe 24.3,

Table 5 Hardness and standard deviation measured by nanoindentation

	Steel	Cu	TiC	TiC/Si	WC/TiC
Mean hardness (GPa)	1.90	11.0	21.8	11.4	19.1
Standard deviation (GPa)	0.28	3.0	2.99	1.21	3.16

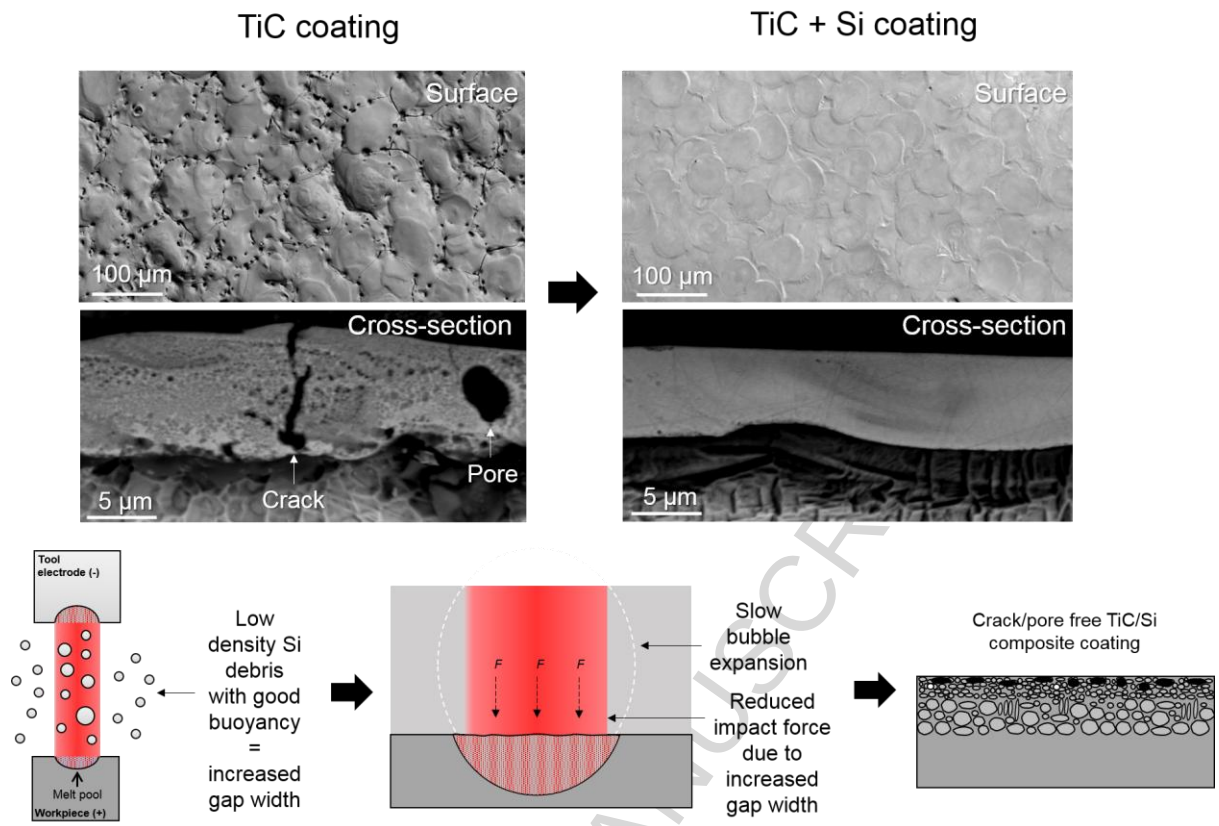

Graphical abstract

Highlights

- A crack/pore free ceramic based coating was made by electrical discharge coating for the first time from sacrificial electrodes.
- A second coating from Si was used to reduced cracking/porosity in a TiC layer via gap width enhancement.
- Material attachment level is correlated with melting point, explained by resistance to ejection via quicker solidification.
- A TiC coating yielded hardness double that of a Cu based recast layer.
- Recast layer removal may be avoided by adoption of multi-layer coatings for favourable mechanical properties.

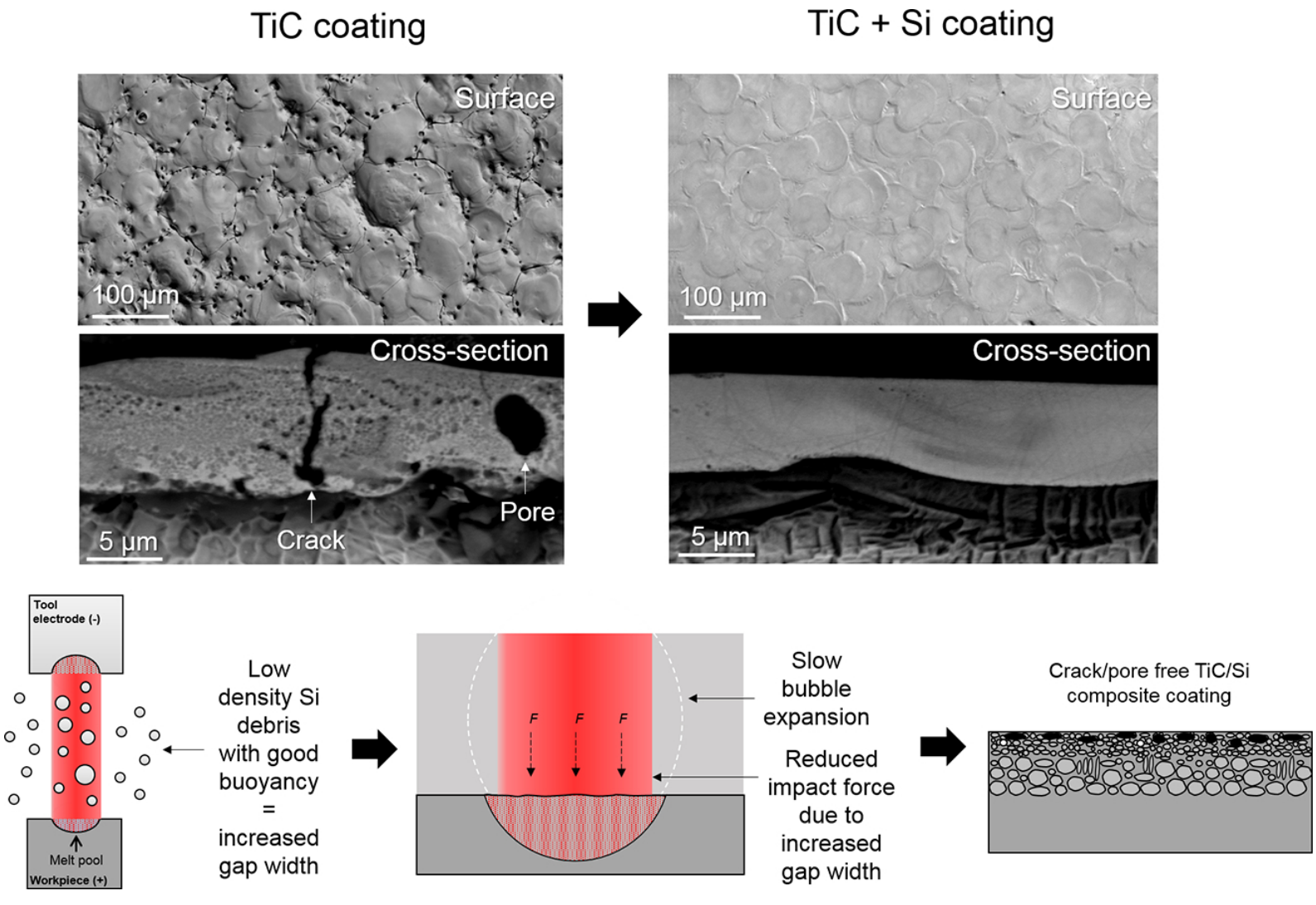

Graphics Abstract

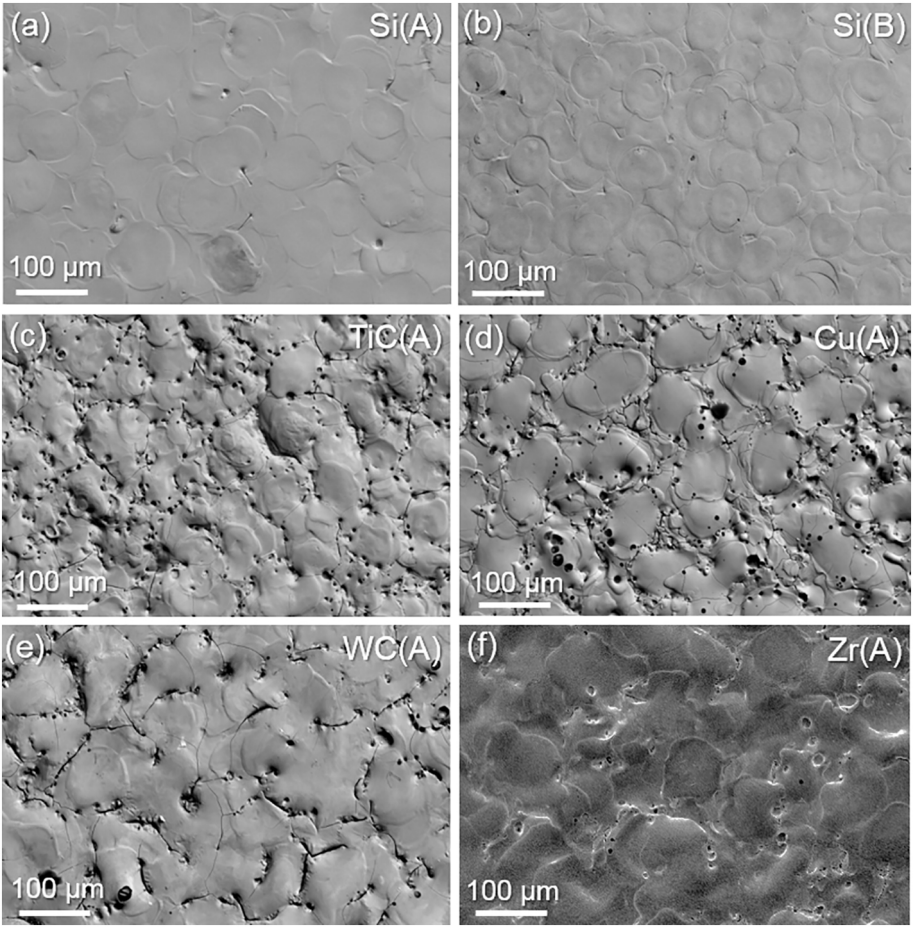
(a)
Si(A)
100 μm
(b)
Si(B)
100 μm
(c)
TiC(A)
100 μm
(d)
Cu(A)
100 μm
(e)
WC(A)
100 μm
(f)
Zr(A)
100 μm

Figure 1

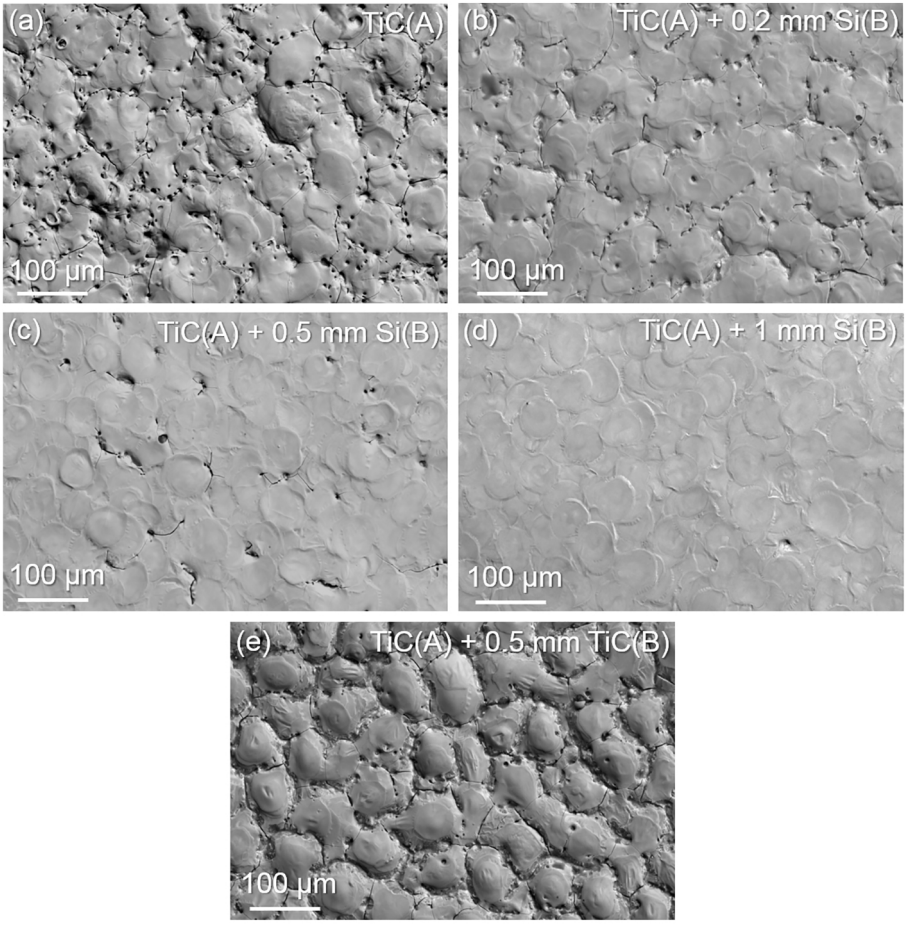
(a)
TiC(A)
100 µm
(b)
TiC(A) + 0.2 mm Si(B)
100 µm
(c)
TiC(A) + 0.5 mm Si(B)
100 µm
(d)
TiC(A) + 1 mm Si(B)
100 µm
(e)
TiC(A) + 0.5 mm TiC(B)
100 µm

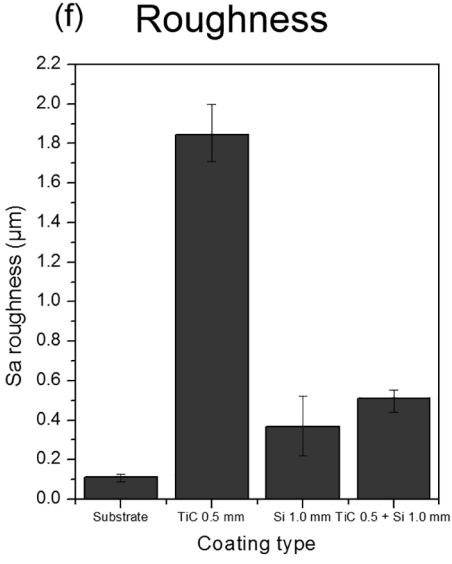
(f) Roughness
Sa roughness (µm)
2.2
2.0
1.8
1.6
1.4
1.2
1.0
0.8
0.6
0.4
0.2
0.0
Substrate
TiC 0.5 mm
Si 1.0 mm
TiC 0.5 + Si 1.0 mm
Coating type

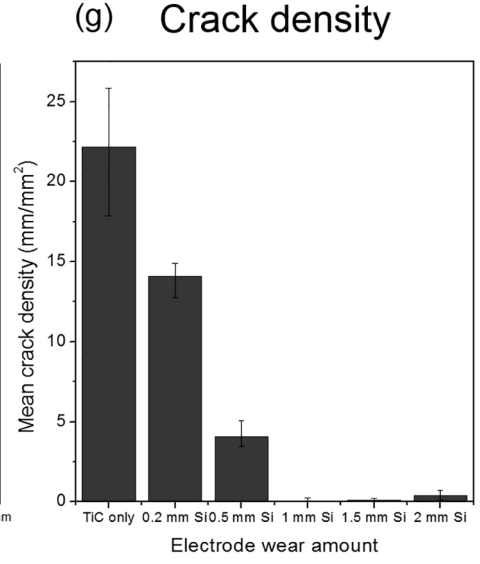
(g) Crack density
Mean crack density (mm/mm²)
25
20
15
10
5
0
TiC only
0.2 mm Si
0.5 mm Si
1 mm Si
1.5 mm Si
2 mm Si
Electrode wear amount

Figure 2

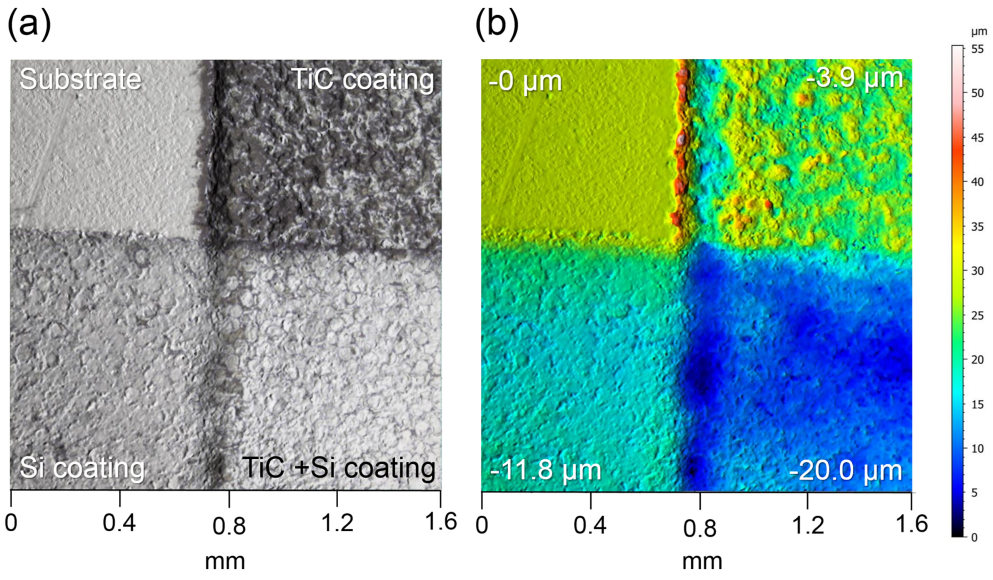
(a)
Substrate
TiC coating
Si coating
TiC +Si coating
0
0.4
0.8
1.2
1.6
mm
(b)
-0 µm
-3.9 µm
-11.8 µm
-20.0 µm
0
0.4
0.8
1.2
1.6
mm
µm
55
50
45
40
35
30
25
20
15
10
5
0

Figure 3

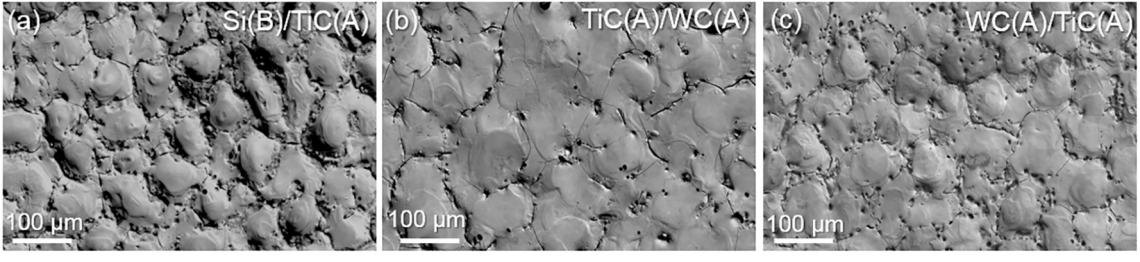

Figure 4

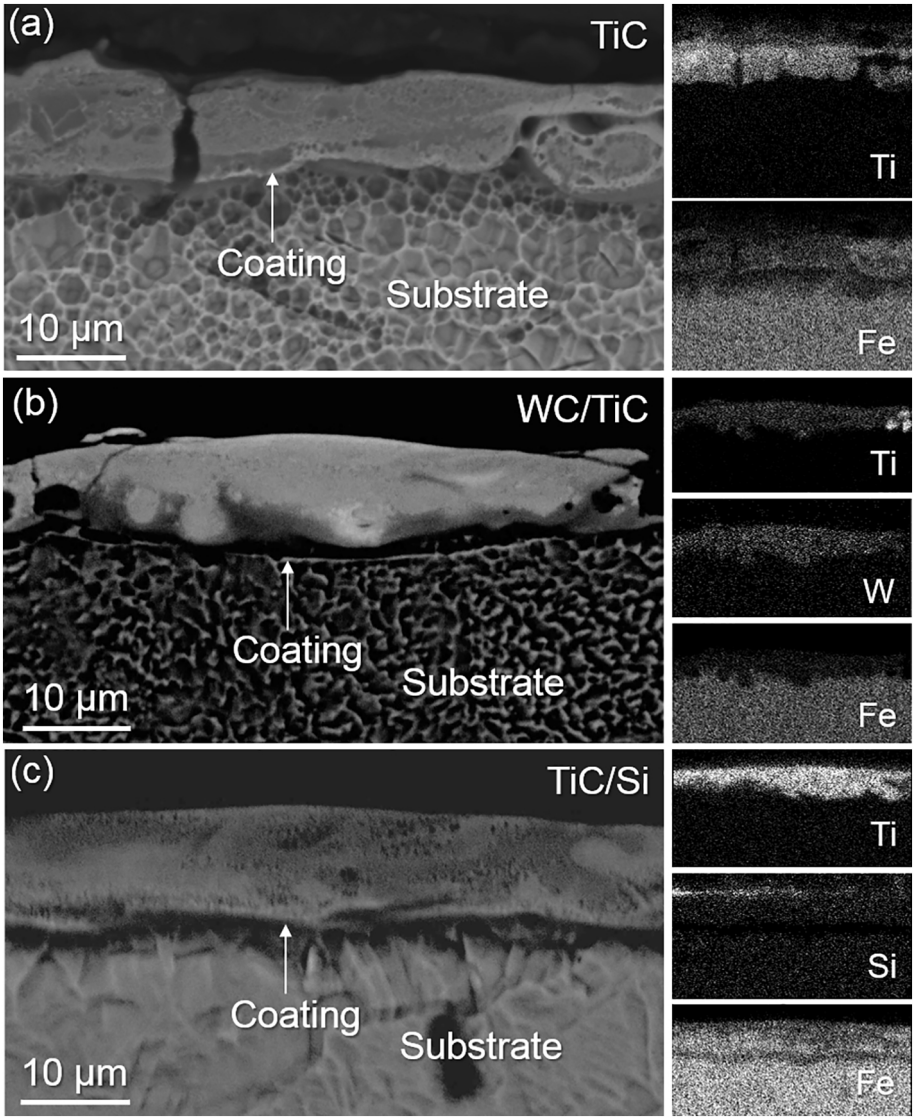
(a)
TiC
Coating
Substrate
10 μm
Ti
Fe
(b)
WC/TiC
Coating
Substrate
10 μm
Ti
W
Fe
(c)
TiC/Si
Coating
Substrate
10 μm
Ti
Si
Fe

Figure 5

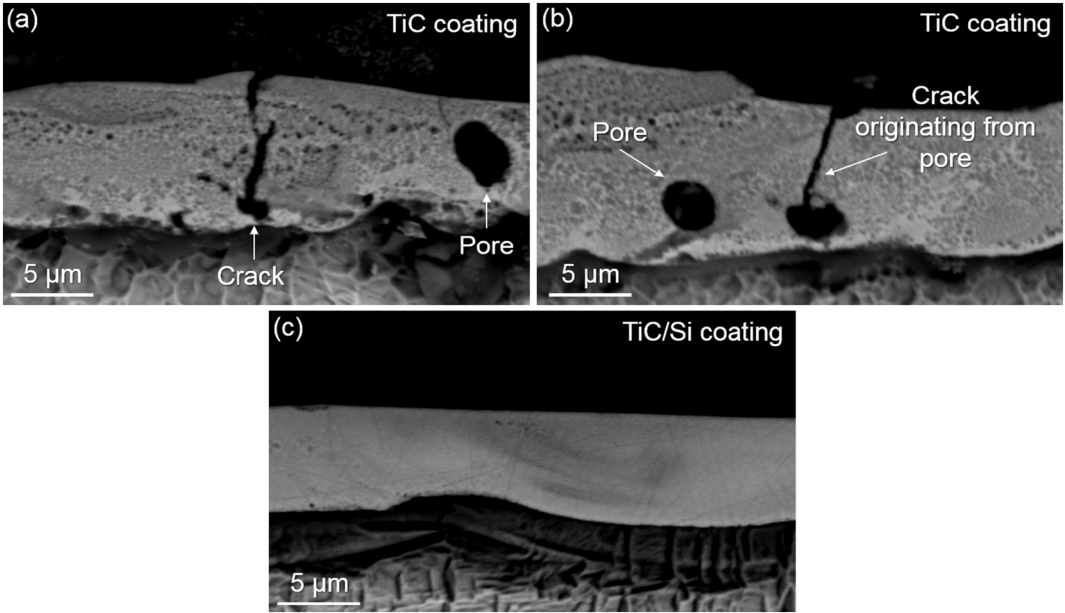
(a)
TiC coating
Pore
Crack
5 µm
(b)
TiC coating
Pore
Crack originating from pore
5 µm
(c)
TiC/Si coating
5 µm

Figure 6

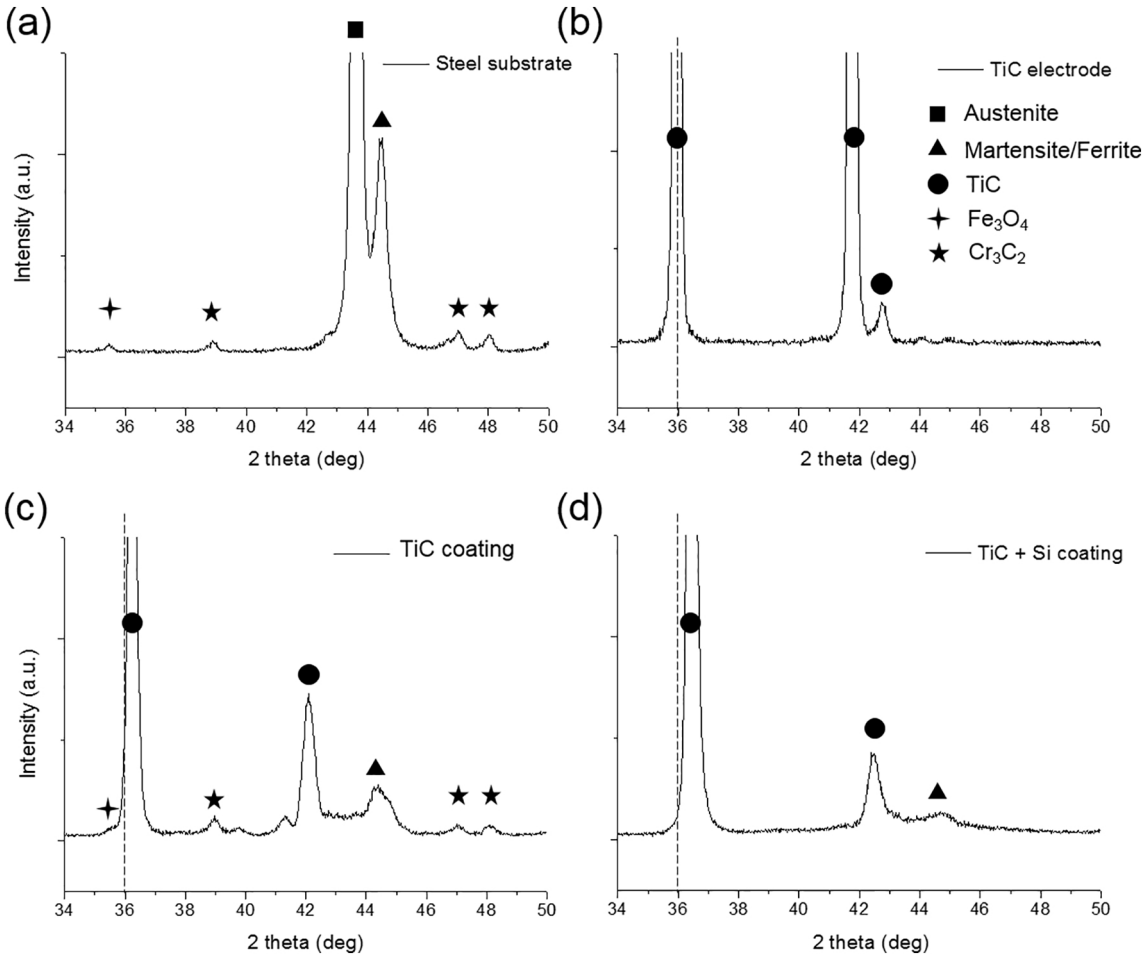
(a)
Steel substrate
Intensity (a.u.)
2 theta (deg)
(b)
TiC electrode
Austenite
Martensite/Ferrite
TiC
Fe_3O_4
Cr_3C_2
2 theta (deg)
(c)
TiC coating
Intensity (a.u.)
2 theta (deg)
(d)
TiC + Si coating
2 theta (deg)

Figure 7

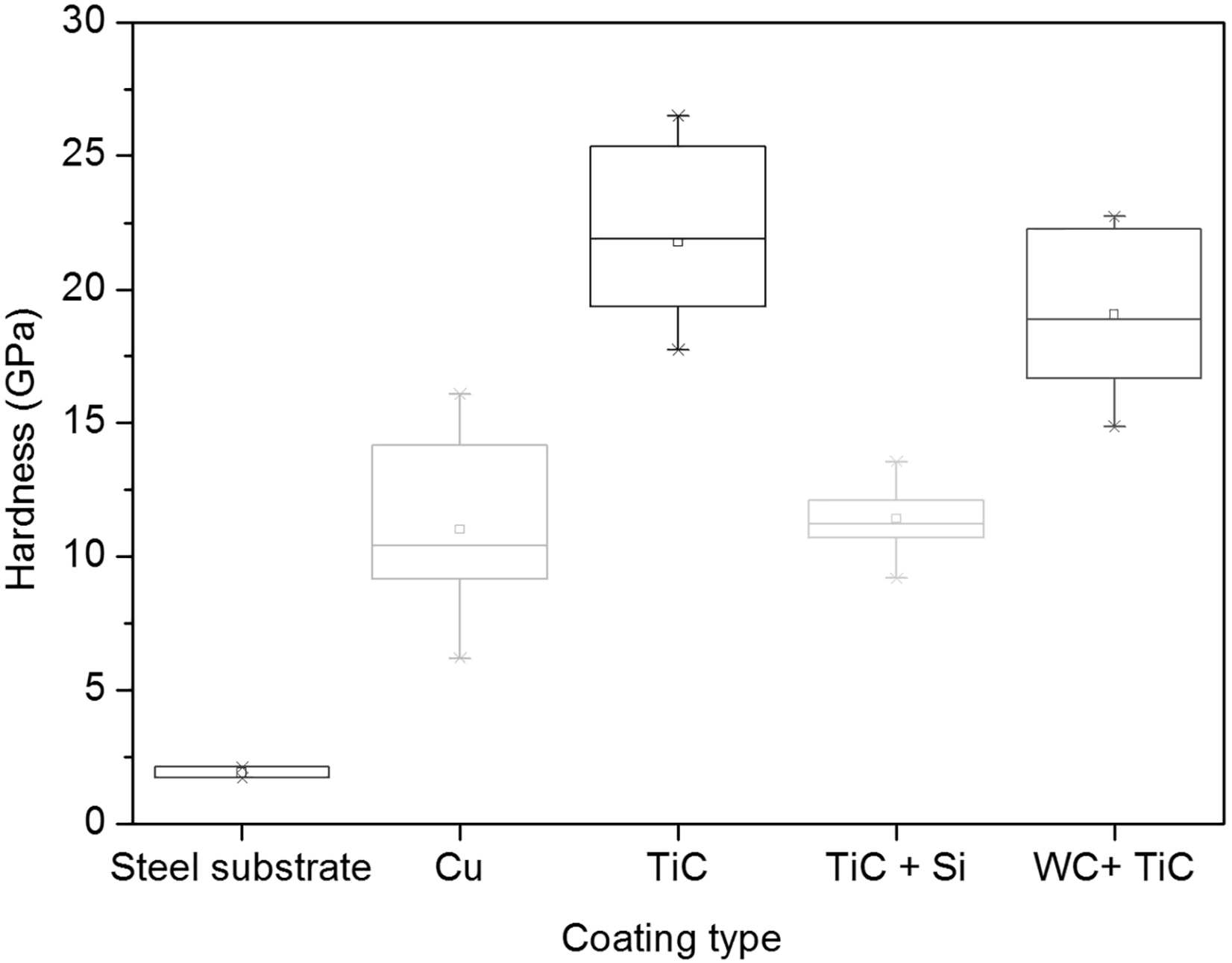
30
25
20
15
10
5
0
Hardness (GPa)
Steel substrate
Cu
TiC
TiC + Si
WC+ TiC
Coating type

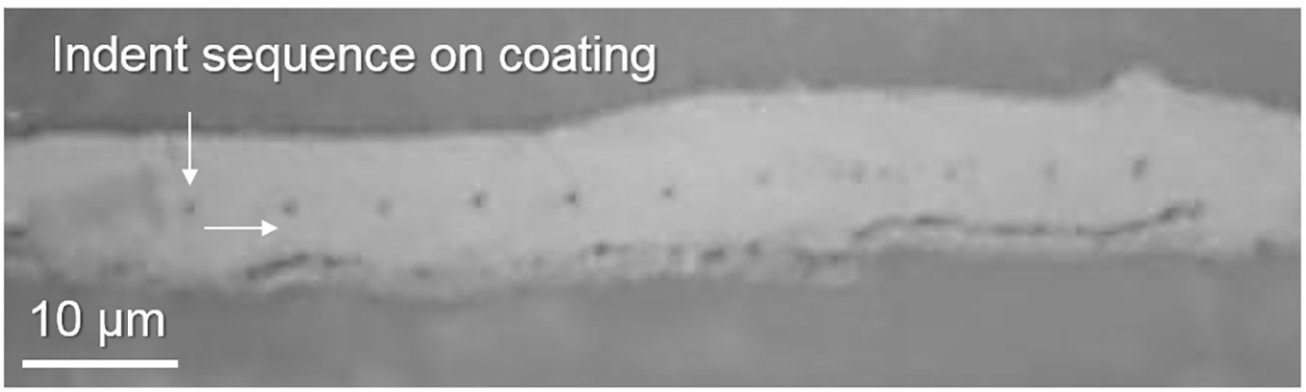
Indent sequence on coating
10 µm

Figure 8

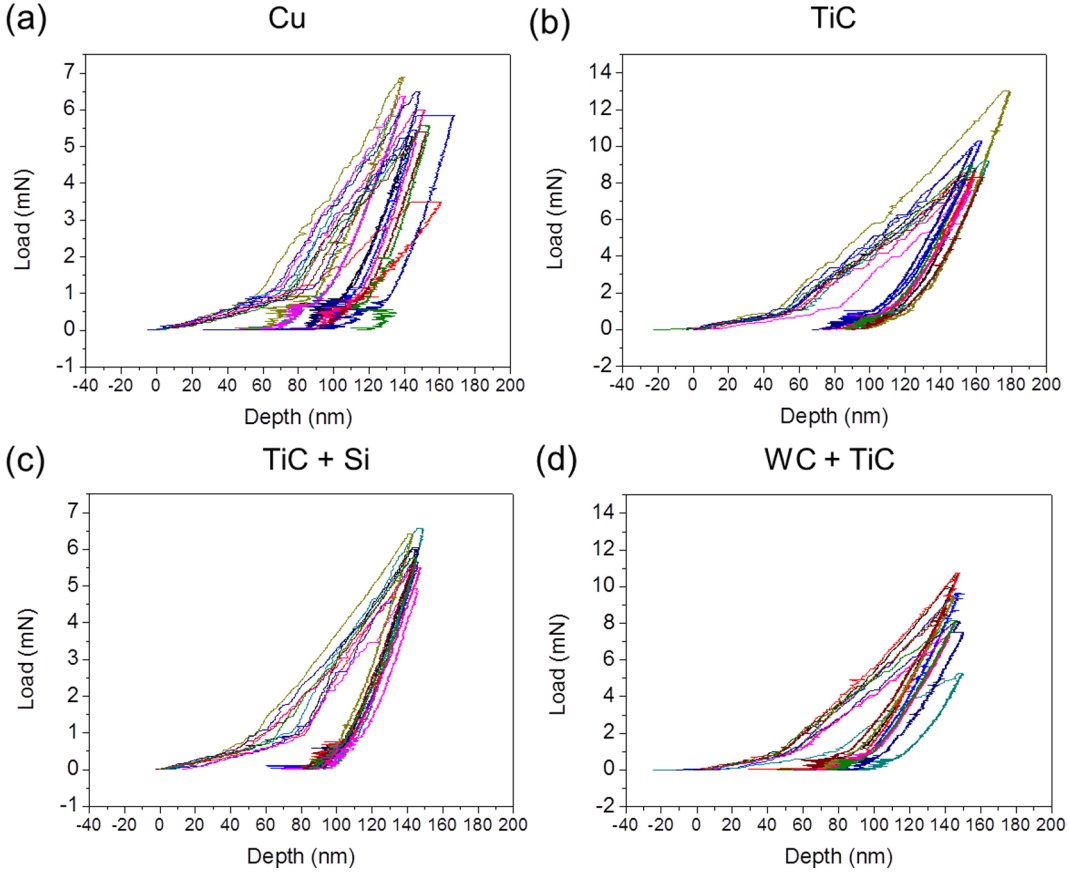
(a)
Cu
Load (mN)
Depth (nm)
(b)
TiC
Load (mN)
Depth (nm)
(c)
TiC + Si
Load (mN)
Depth (nm)
(d)
WC + TiC
Load (mN)
Depth (nm)

Figure 9

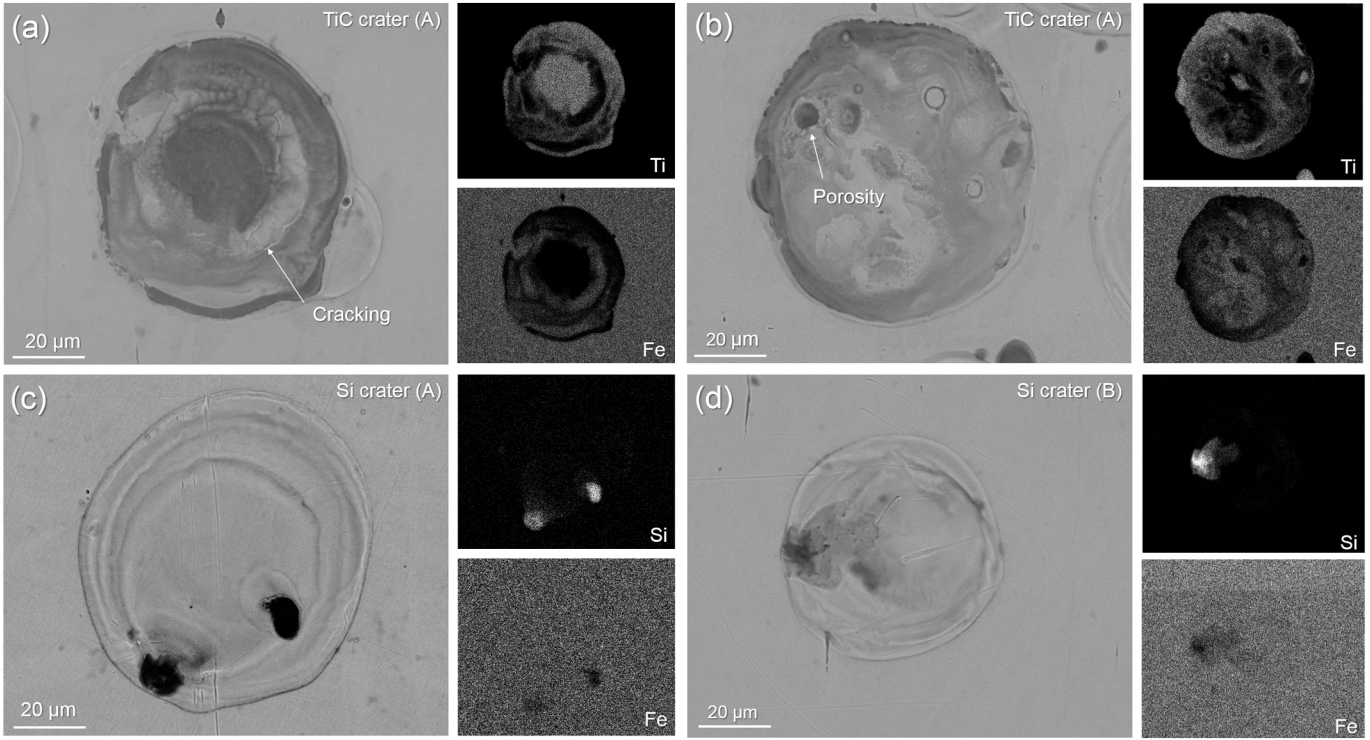
(a)
TiC crater (A)
Cracking
20 µm
Ti
Fe
(b)
TiC crater (A)
Porosity
20 µm
Ti
Fe
(c)
Si crater (A)
20 µm
Si
Fe
(d)
Si crater (B)
20 µm
Si
Fe

Figure 10

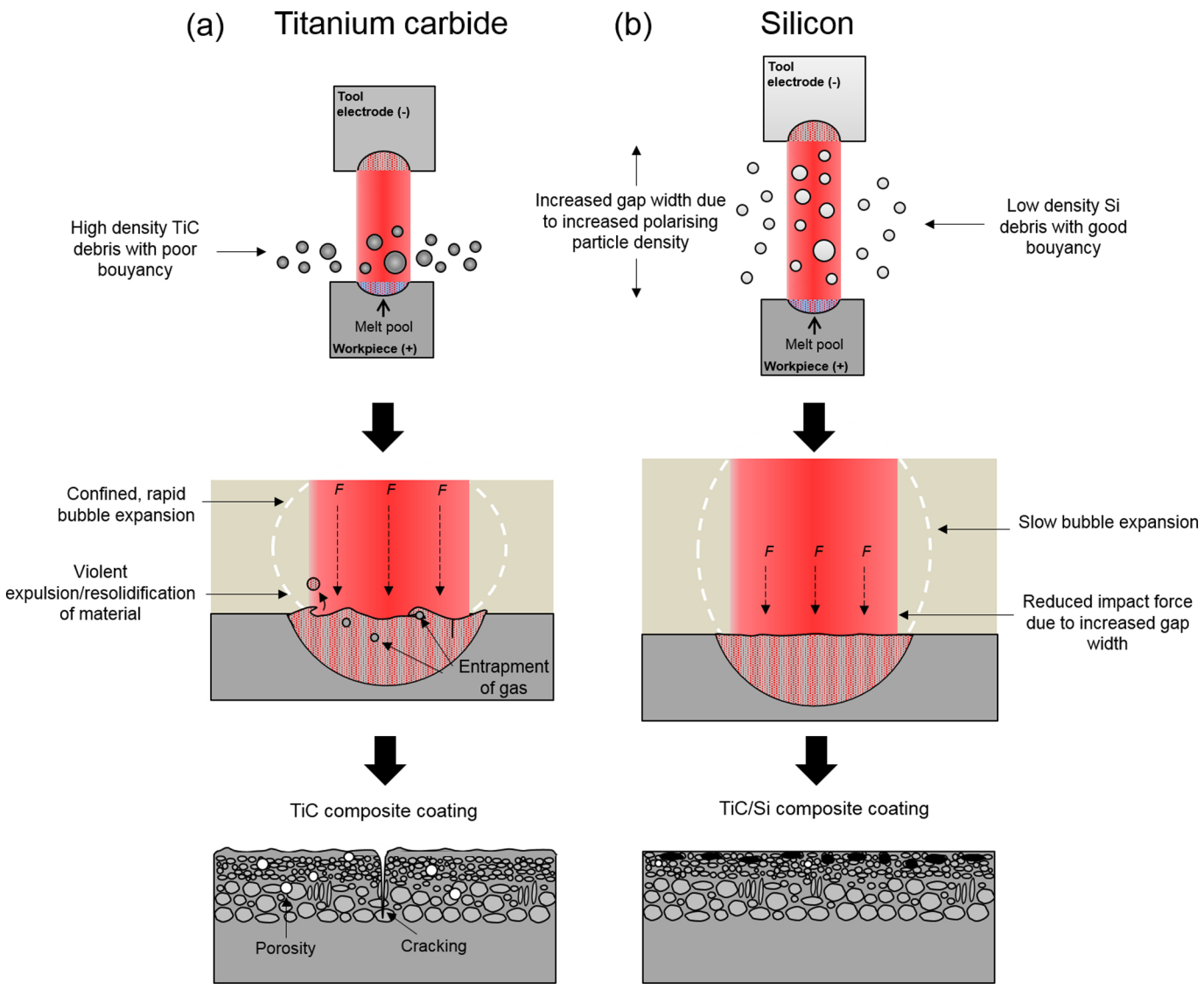
(a) Titanium carbide
(b) Silicon
Tool electrode (-)
High density TiC debris with poor bouyancy
Melt pool
Workpiece (+)
Increased gap width due to increased polarising particle density
Low density Si debris with good bouyancy
Confined, rapid bubble expansion
Violent expulsion/resolidification of material
F
Entrapment of gas
Slow bubble expansion
Reduced impact force due to increased gap width
TiC composite coating
TiC/Si composite coating
Porosity
Cracking

Figure 11

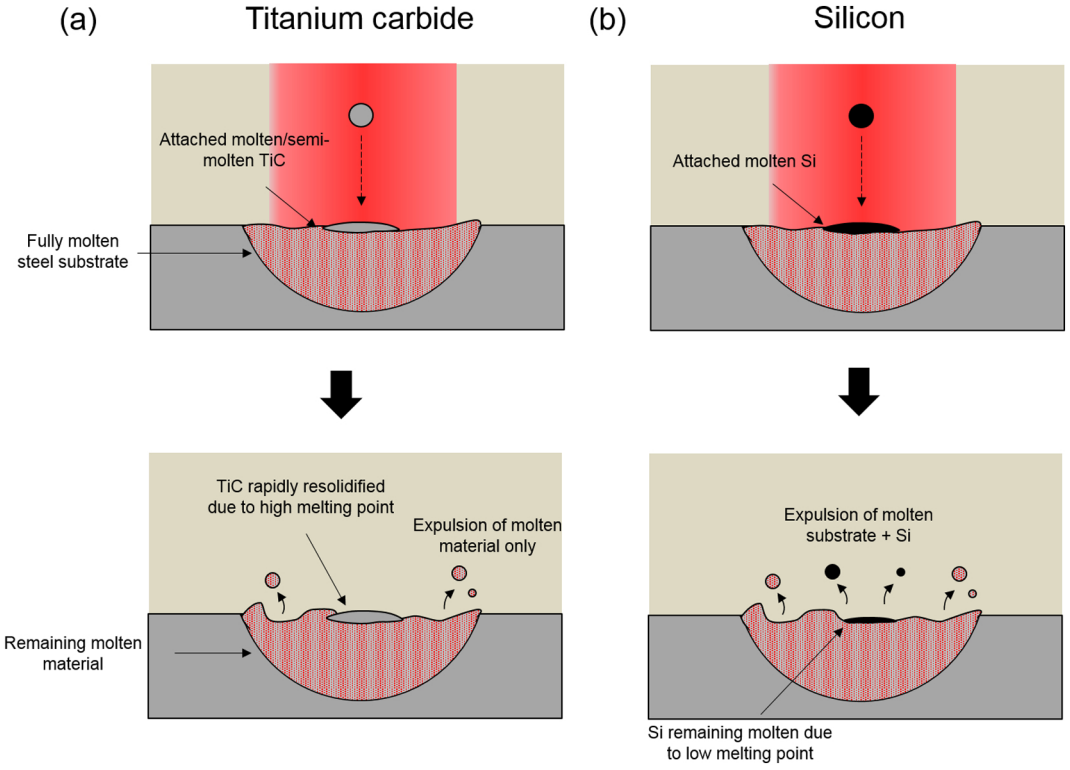
(a)
Titanium carbide
(b)
Silicon
Attached molten/semi-molten TiC
Attached molten Si
Fully molten steel substrate
TiC rapidly resolidified due to high melting point
Expulsion of molten material only
Expulsion of molten substrate + Si
Remaining molten material
Si remaining molten due to low melting point

Figure 12